Cross-talk between N-terminal and C-terminal domains in stromal interaction molecule 2 (STIM2) determines enhanced STIM2 sensitivity

Received for publication, December 17, 2018, and in revised form, February 28, 2019 Published, Papers in Press, March 1, 2019, DOI 10.1074/jbc.RA118.006801

Scott M. Emrich[‡1], Ryan E. Yoast[‡1], Ping Xin[‡], Xuexin Zhang[‡], Trayambak Pathak[‡], Robert Nwokonko[‡], Maxime F. Gueguinou[‡], Krishna P. Subedi[§], Yandong Zhou[‡], Indu S. Ambudkar[§], Nadine Hempel[¶], Khaled Machaca[‖], Donald L. Gill[‡], and Mohamed Trebak[‡2]

From the Departments of [‡]Cellular and Molecular Physiology and [¶]Pharmacology, Pennsylvania State University College of Medicine, Hershey, Pennsylvania 17033, the [§]Secretory Physiology Section, NIDCR, National Institutes of Health, Bethesda, Maryland 20892, and the [‖]Department of Physiology and Biophysics, Weill Cornell Medical College in Qatar, Education City, Qatar Foundation, P.O. Box 24144, Doha, Qatar

Edited by Roger J. Colbran

Store-operated Ca^{2+} entry (SOCE) is a ubiquitous pathway for Ca^{2+} influx across the plasma membrane (PM). SOCE is mediated by the endoplasmic reticulum (ER)-associated Ca^{2+}-sensing proteins stromal interaction molecule 1 (STIM1) and STIM2, which transition into an active conformation in response to ER Ca^{2+} store depletion, thereby interacting with and gating PM-associated ORAI1 channels. Although structurally homologous, STIM1 and STIM2 generate distinct Ca^{2+} signatures in response to varying strengths of agonist stimulation. The physiological functions of these Ca^{2+} signatures, particularly under native conditions, remain unclear. To investigate the structural properties distinguishing STIM1 and STIM2 activation of ORAI1 channels under native conditions, here we used CRISPR/Cas9 to generate STIM1$^{-/-}$, STIM2$^{-/-}$, and STIM1/2$^{-/-}$ knockouts in HEK293 and colorectal HCT116 cells. We show that depending on cell type, STIM2 can significantly sustain SOCE in response to maximal store depletion. Utilizing the SOCE modifier 2-aminoethoxydiphenyl borate (2-APB), we demonstrate that 2-APB–activated store-independent Ca^{2+} entry is mediated exclusively by endogenous STIM2. Using variants that either stabilize or disrupt intramolecular interactions of STIM C termini, we show that the increased flexibility of the STIM2 C terminus contributes to its selective store-independent activation by 2-APB. However, STIM1 variants with enhanced flexibility in the C terminus failed to support its store-independent activation. STIM1/STIM2 chimeric constructs indicated that coordination between N-terminal sensitivity and C-terminal flexibility is required for specific store-independent STIM2 activation. Our results clarify the structural determinants underlying activation of specific STIM isoforms, insights that are potentially useful for isoform-selective drug targeting.

In nonexcitable cells, cytosolic Ca^{2+} concentrations are controlled through release from intracellular Ca^{2+} stores of the endoplasmic reticulum (ER)[3] and Ca^{2+} influx across the plasma membrane (PM) through the ubiquitous store-operated Ca^{2+} entry (SOCE) pathway (1). SOCE is required for the acute refilling of ER Ca^{2+} stores and sustaining downstream signaling to gene transcription in most cell types (2–5). SOCE is mediated by the ER Ca^{2+} sensors stromal interaction molecules (STIM1 and STIM2), which directly bind, cross-link, and gate plasma membrane ORAI1 channels in response to store depletion. Extensive investigation into the molecular interactions between STIM1 and ORAI1 has revealed STIM1 as a potent activator of ORAI1 channels through a strategically positioned phenylalanine (Phe-394) located within the STIM-ORAI–activating region (SOAR1) in the STIM1 C terminus (6–8). Furthermore, the N-terminal EF-hand domain of STIM1 located within the ER lumen has a high affinity for Ca^{2+}, requiring significant depletion of ER Ca^{2+} stores for the transition of STIM1 into an active conformation (9, 10). In contrast, the structurally homologous STIM2 is a relatively weak activator of ORAI1, in which the residue equivalent to Phe-394 of STIM1 is a leucine (Leu-485) within the SOAR domain of STIM2 (SOAR2) that renders it a partial agonist (6). The luminal N-terminal EF-hand domain of STIM2 has a lower affinity for Ca^{2+} compared with STIM1, allowing STIM2 to sense minor reductions in ER Ca^{2+} concentrations (11). As a result, a significant pool of STIM2 protein appears to be constitutively active and bound to ORAI1 channels, possibly as a mechanism to maintain basal cytosolic and ER Ca^{2+} concentrations (11, 12). Interestingly, a previous study proposed that the short N-terminal peptide before the EF-hand domain in STIM2 functions as "brake" to ensure negative regulation of STIM2 constitutive activity and prevent significant enhancement of basal cytosolic Ca^{2+}

This work was supported by National Institutes of Health Grants R01HL123364, R01HL097111, and R21AG050072 (to M. T.), Grants R01GM120783 and R01GM109279 (to D. L. G.), and Qatar National Research Fund (QNRF) Grant NPRP8-110-3-021 (to M. T. and K. M.). The authors declare that they have no conflicts of interest with the contents of this article. The content is solely the responsibility of the authors and does not necessarily represent the official views of the National Institutes of Health.

[1] Both authors contributed equally to this work.

[2] To whom correspondence should be addressed. E-mail: mtrebak@psu.edu.

[3] The abbreviations used are: ER, endoplasmic reticulum; STIM, stromal interaction molecule; SOCE, store-operated Ca^{2+} entry; SOAR, STIM-ORAI activating region; OASF, ORAI activating small fragment; 2-APB, 2-aminoethoxydiphenyl borate; PM, plasma membrane; TM, transmembrane; BisTris, 2-[bis(2-hydroxyethyl)amino]-2-(hydroxymethyl)propane-1,3-diol; GAPDH, glyceraldehyde-3-phosphate dehydrogenase; YFP, yellow fluorescent protein; CFP, cyan fluorescent protein; aa, amino acid(s); CCmt, coiled-coil 1/coiled-coil 3 mutant.

concentration (13). A recent report further showed that the E470G mutation within the SOAR2 domain of STIM2 (Glu-470 is equivalent to Gly-379 in STIM1) renders STIM2 a fast and robust activator of ORAI1, whereas the opposite mutation in STIM1 only weakly activates ORAI1 (14). The same group showed that the transmembrane (TM) domain of STIM2 contributes to its slow activation kinetics compared with STIM1 (14). Although STIM1 has been shown to drive the majority of SOCE in a variety of cell types in response to agonist-induced store depletion (9, 15–17), the physiological function of STIM2 in this process is not clear. Further adding to the complexity of this system is recent evidence demonstrating that STIM2 plays a role in inducing the active conformation of STIM1 and regulating its coupling with ORAI1 channels under conditions of replete ER Ca^{2+} stores (18, 19). The physiological implications of this mechanism, particularly how endogenous STIM proteins utilize this molecular coordination to drive cell function, are unknown. Additionally, the structural differences between STIM1 and STIM2 that determine their differential response to varying strengths of agonist and the distinct roles of STIM1 and STIM2 in cell physiology, especially under native conditions, are largely unknown.

Multiple classes of pharmacological compounds that either enhance or inhibit SOCE activity have been identified (20, 21). Among these SOCE channel modifiers, the compound 2-aminoethoxydiphenyl borate (2-APB) has been well characterized and widely utilized (22–24). 2-APB displays a unique biphasic effect on ORAI1 activity, potentiating it at low concentrations (1–10 μM) and inhibiting it at high concentrations (~30–50 μM) (25). High concentrations of 2-APB have been demonstrated to: 1) inhibit several constitutively active STIM-independent ORAI1 channel mutants, whereas potentiating WT ORAI3, suggesting that 2-APB acts directly on ORAI channel pore; 2) strengthen intramolecular interaction within the STIM1 C terminus, between the coiled-coil 1 (CC1) domain and SOAR1, thus preventing STIM1 unfolding in response to store depletion. This would result in a reduction in STIM1 oligomerization and puncta formation that would reduce functional interactions with ORAI1 (22, 26–31). However, the ability of 2-APB at low concentrations to selectively increase Ca^{2+} influx through ORAI1 channels remains enigmatic.

Although 2-APB is relatively nonspecific and can affect a diverse array of ion channels, a clear understanding of how 2-APB interacts with and regulates ORAI and STIM proteins under native levels of expression would be crucial for the future development of potent and selective SOCE modifying compounds (32–34). Here, we generated multiple cell lines using CRISPR/Cas9 technology that are devoid of individual STIM proteins ($STIM1^{-/-}$, $STIM2^{-/-}$) as well as double STIM1 and STIM2 knockout cells ($STIM1/2^{-/-}$). Our results demonstrate that store-independent activation of SOCE with low concentrations of 2-APB (10 μM) occurs exclusively through endogenous STIM2. Through the use of chimeric STIM proteins and STIM mutant constructs, we clearly demonstrate that the effects of 2-APB on STIM2 requires the combination of increased flexibility of the STIM2 C terminus and increased sensitivity of its N-terminal EF-hand. Thus, the use of low concentrations of 2-APB as a pharmacological tool to selectively drive native STIM2-mediated Ca^{2+} entry provides a novel strategy to dissect the physiological functions of STIM2 under homeostatic and endogenous conditions. Furthermore, development of 2-APB–derived analogues with increased specificity and potency for STIM2 will selectively target cellular pathways that rely on STIM2 in both healthy and disease conditions.

Results

Generation and characterization of $STIM1^{-/-}$, $STIM2^{-/-}$, and $STIM1/2^{-/-}$ knockout cell lines

We utilized CRISPR/Cas9 technology to delete each STIM protein individually and in combination in HEK293 cells. Western blot analysis of HEK293 $STIM1^{-/-}$ and $STIM2^{-/-}$ cell lines demonstrated no compensatory up-regulation of STIM1 or STIM2 proteins in response to individual STIM knockout, whereas $STIM1/2^{-/-}$ cells were devoid of both proteins (Fig. 1, *A* and *B*). Fura-2 Ca^{2+} imaging was performed in each HEK293 knockout cell line to measure SOCE in response to store depletion with the sarco/endoplasmic reticulum Ca^{2+}-ATPase (SERCA) pump inhibitor thapsigargin (Fig. 1, *C* and *D*). HEK293 $STIM1^{-/-}$ cells exhibit substantial inhibition in peak SOCE (to ~10% of WT), whereas $STIM2^{-/-}$ cells showed only minor reduction in peak SOCE (~84% of WT). Knockout of both STIM1 and STIM2 (HEK293 $STIM1/2^{-/-}$ cells) results in essentially complete abrogation of SOCE (~3% of WT) upon re-addition 2 mM Ca^{2+} to the extracellular medium. To investigate cell type-dependent contributions of STIM1 *versus* STIM2 to Ca^{2+} signals, we also generated individual STIM1 and STIM2 knockout of the colorectal cancer cell line HCT116 and documented knockouts with Western blots (Fig. 1, *E* and *F*). Ca^{2+} imaging experiments demonstrated a significant reduction in peak SOCE in HCT116 $STIM1^{-/-}$ cells (~24% of WT) (Fig. 1, *G* and *H*). Interestingly, HCT116 $STIM2^{-/-}$ cells also showed substantial reduction in SOCE (~44% of WT) despite having STIM1 protein present. These results suggest that STIM2 plays differential, cell type-specific role in supporting SOCE in response to maximal ER store depletion.

2-APB activates store-independent Ca^{2+} entry exclusively through STIM2

Using our newly generated HEK293 and HCT116 STIM knockout cell lines, we investigated the effects of low (10 μM) and high (50 μM) 2-APB under conditions where internal Ca^{2+} stores were replete. To address potential off target effects of CRISPR/Cas9, we generated additional STIM1 and STIM2 knockout clones in both cell lines using multiple guide RNA sequences (Fig. 2, *A* and *F*). Our results presented in detail below show that STIM2, but not STIM1, is crucial for 2-APB-activated Ca^{2+} entry. To strengthen this argument, we present data obtained from 4 $STIM2^{-/-}$ HCT116 cell clones representing 2 independent clones each obtained from two independent guide RNA (*e.g.* $STIM2^{-/-}$g1.1 corresponds to clone 1 from guide RNA 1 etc.; Fig. 2*F*). Stimulation of WT HEK293 and HEK $STIM1^{-/-}$ cells with 10 μM 2-APB in the presence of 2 mM extracellular Ca^{2+} demonstrated a gradual and sustained increase in cytosolic Ca^{2+} concentrations (Fig. 2, *B* and *C*). Importantly, this potentiation was not observed in HEK $STIM2^{-/-}$ or $STIM1/2^{-/-}$ cell lines, strongly arguing that

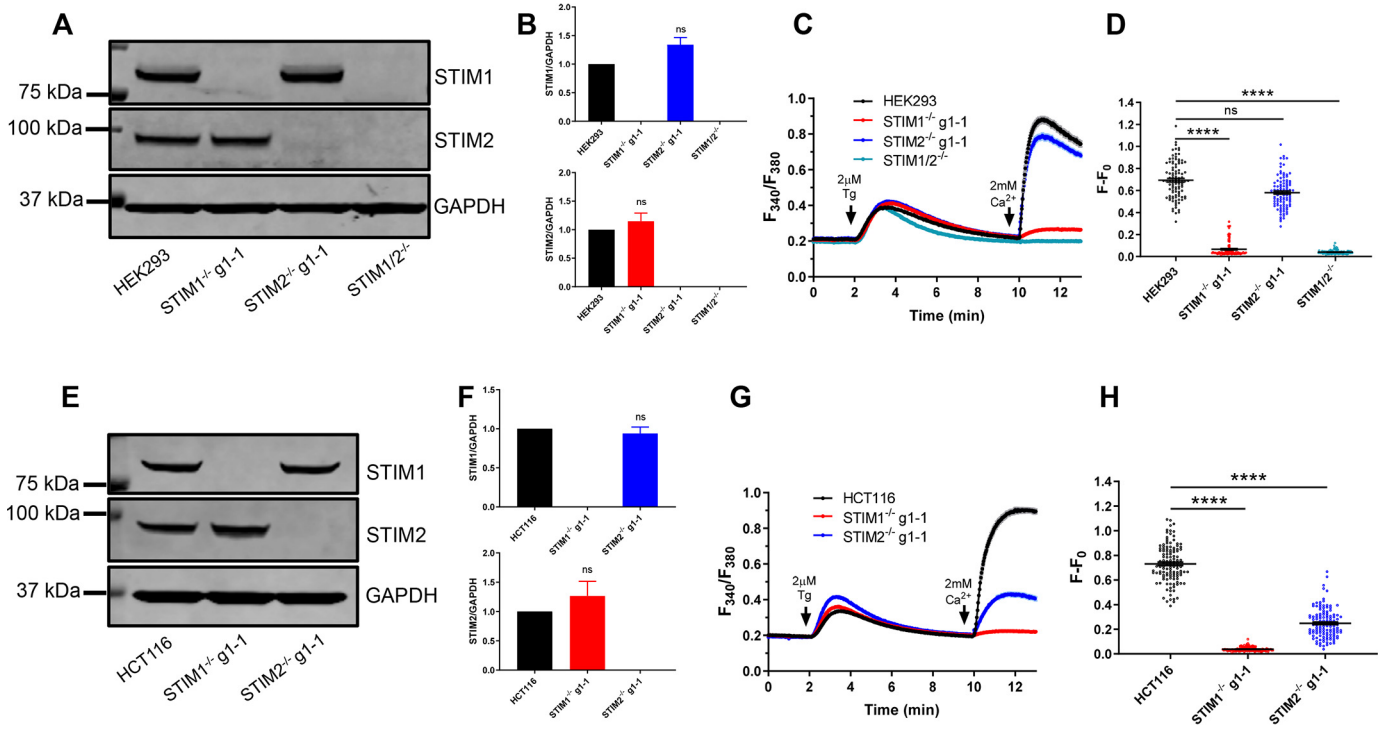

Figure 1. Generation and characterization of STIM1, STIM2, and STIM1/STIM2 knockout cell lines. *A,* Western blot analysis of STIM1, STIM2, and the loading control GAPDH in HEK293 wildtype (*WT*) cells, STIM1$^{-/-}$, STIM2$^{-/-}$, and STIM1/2$^{-/-}$ cells. Blots are representative of 3 independent experiments and intensity of STIM bands normalized to GAPDH are quantified in *B*. *C,* representative cytosolic Ca^{2+} traces in different HEK293 cells as measured by Fura-2 in response to store depletion with 2 μM thapsigargin (*Tg*) in nominally Ca^{2+}-free external solution and subsequent re-introduction of 2 mM Ca^{2+} to the extracellular medium. All traces are represented as mean (*dark symbols*) ± S.E. (*light background shading*). *D,* peak SOCE calculated as the baseline-subtracted maximal values of Fura-2 ratio units. Each scatter plot displays distribution of peak SOCE values for $n = 100$ cells from a total of 3 independent experiments. *E,* Western blot analysis of STIM1, STIM2, and the loading control GAPDH in WT HCT116 cells, STIM1$^{-/-}$, and STIM2$^{-/-}$ cells. Blots are representative of 3 independent experiments and densitometry of STIM bands normalized to GAPDH are quantified in *F*. *G,* representative Ca^{2+} imaging traces in different HCT116 cells using the same protocol as in *C*. *H,* peak SOCE calculated as in *D*. Each scatter plot displays distribution of peak SOCE values for $n = 100$ cells from a total of 3 independent experiments. ****, $p < 0.0001$, Kruskal-Wallis test with Dunn's multiple comparisons to WT parental line.

STIM2 is the target of 2-APB store-independent activation of Ca^{2+} entry. Similar to HEK293 cells, stimulation of HCT116 WT and STIM1$^{-/-}$ cells with 10 μM 2-APB demonstrated a small yet sustained Ca^{2+} entry, which was not observed in HCT116 STIM2$^{-/-}$ cells (Fig. 2, *G* and *H*). Addition of 50 μM 2-APB to different variants of HEK293 cells showed a marginal and transient increase in cytosolic Ca^{2+} (Fig. 2, *D* and *E*). Surprisingly, stimulation of WT HCT116 cells with 50 μM 2-APB showed a more pronounced, rapid and transient increase in cytosolic Ca^{2+}, and this effect was further enhanced in HCT116 STIM1$^{-/-}$ cells (Fig. 2, *I* and *J*). This rapid potentiation with 50 μM 2-APB was not observed in HCT116 STIM2$^{-/-}$ cells (Fig. 2, *I* and *J*). These results suggest that 2-APB activates endogenous STIM2, but not STIM1, in both cell lines in a store-independent manner and that the more potent activation of Ca^{2+} entry by 50 μM 2-APB in HCT116 cells results from the more prominent role STIM2 plays in SOCE of HCT116 cells.

Previous studies showed that overexpression of wildtype (WT) STIM2 in WT HEK293 cells results in pre-clustered STIM2 puncta located at junctions between the ER and plasma membrane in the absence of store depletion (11). Here, we utilized HEK293 STIM1/2$^{-/-}$ cells with a clean genetic background lacking endogenous STIM proteins. When expressed in STIM1/2$^{-/-}$ HEK293 cells, YFP-tagged STIM2 displayed significant puncta formation throughout the entirety of the cell under basal conditions (Fig. 3*A*). Although treatment with 10 μM 2-APB caused a reduction in cell size and reorganization of STIM2 puncta, it did not lead to significant enhancement of puncta size from baseline (Fig. 3*B*). In contrast, overexpressed STIM1 protein displayed a diffuse, tubular distribution (Fig. 3*A*), and STIM1 did not form puncta in response to 10 μM 2-APB (Fig. 3*A*). To compare the behavior of native *versus* overexpressed STIMs, Ca^{2+} measurements were performed comparatively in four different groups of HEK293 cells: 1) STIM1/2$^{-/-}$ cells overexpressing STIM2; 2) STIM1/2$^{-/-}$ cells overexpressing STIM1; 3) STIM1$^{-/-}$ cells; and 4) STIM2$^{-/-}$ cells. Direct addition of 10 μM 2-APB to STIM1/2$^{-/-}$ cells overexpressing STIM2 induced a large and sustained store-independent increase in cytosolic Ca^{2+} concentrations (Fig. 3, *C* and *D*). Addition of 10 μM 2-APB to STIM1/2$^{-/-}$ cells overexpressing STIM1 caused store-independent Ca^{2+} entry comparable in magnitude to that observed in HEK293 STIM1$^{-/-}$ cells with endogenous STIM2 (Fig. 3, *C* and *D*). Similar results were observed in response to 50 μM 2-APB stimulation, with STIM1/2$^{-/-}$ cells overexpressing STIM2 demonstrating a rapid and transient store-independent increase in cytosolic Ca^{2+} (Fig. 3, *E* and *F*). Overexpression of STIM1 in STIM1/2$^{-/-}$ cells yielded a marginal increase in cytosolic Ca^{2+} with 50 μM 2-APB stimulation.

Depletion of intracellular Ca^{2+} stores induces rapid puncta formation of STIM1 and induces clustering with ORAI1 channels (7, 35). High concentrations of 2-APB (50 μM) inhibit the formation of STIM1 puncta by clamping the STIM1 C terminus

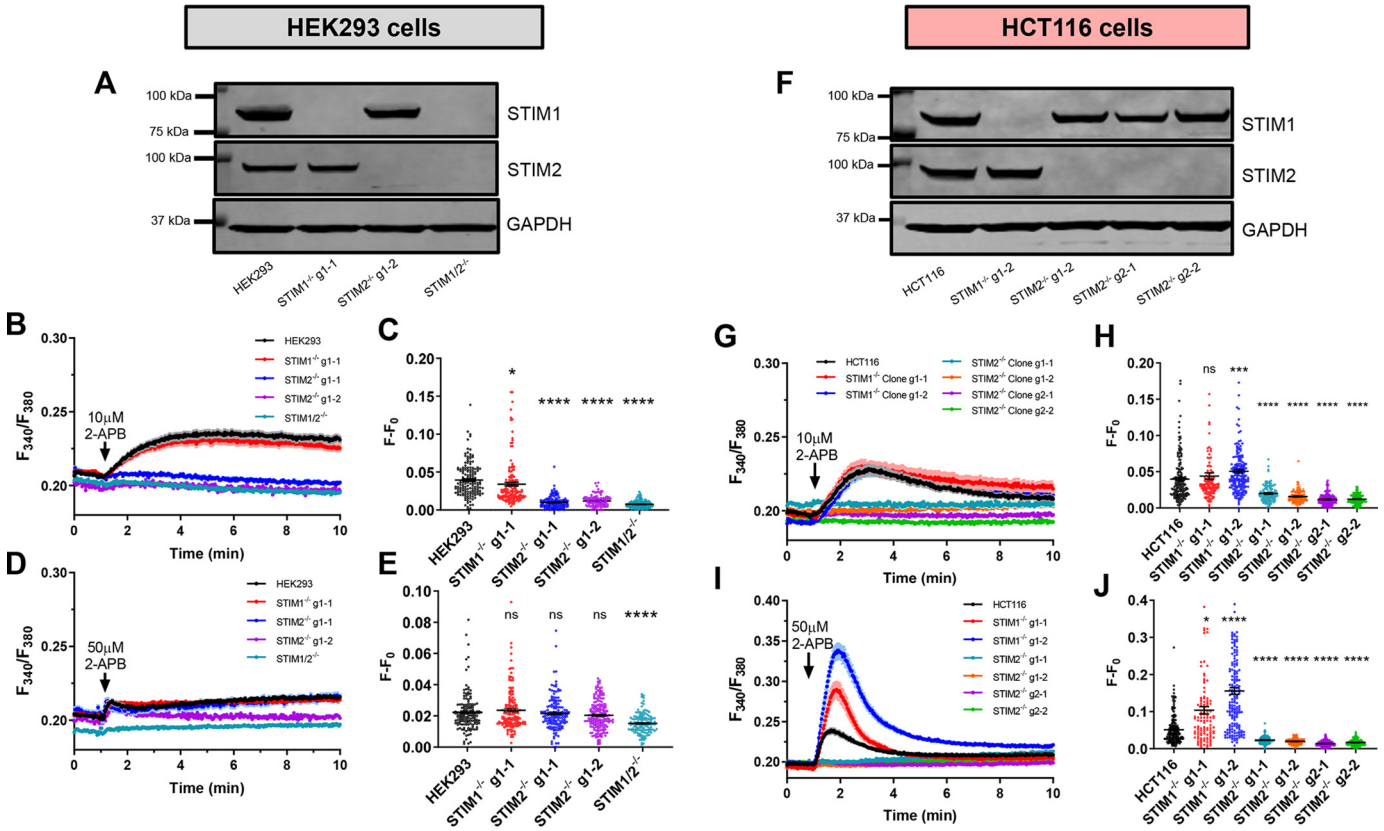

Figure 2. 2-APB activates store-independent Ca^{2+} entry exclusively through endogenous STIM2. *A,* Western blot analysis of STIM1, STIM2, and the loading control GAPDH in additional HEK293 STIM2$^{-/-}$ clones. *B,* Ca^{2+} entry was measured using Fura-2 upon addition of 10 μM 2-APB in the presence of 2 mM Ca^{2+} in WT HEK293 and each STIM CRISPR cell line. Ca^{2+} imaging traces are average data from $n = 145–154$ individual cells/condition. *C,* scatter plots show mean ± S.E. of baseline-subtracted maximal values of Fura-2 ratio units. *D,* Ca^{2+} entry measured upon addition of 50 μM 2-APB. Ca^{2+} imaging traces are average data from $n = 131–150$ individual cells/condition. *E,* scatter plots show mean ± S.E. of baseline-subtracted maximal value of Fura-2 ratio units. *F,* Western blot analysis of STIM1, STIM2, and the loading control GAPDH in additional HCT116 STIM1$^{-/-}$ and STIM2$^{-/-}$ clones. For STIM2$^{-/-}$, clones were generated with 2 distinct guide RNAs (see "Experimental procedures"), with 2 independent clones per guide RNA. *G–J,* same experimental conditions as in *B–E,* except that WT HCT116 and its STIM CRISPR cell line variants were used. *G,* 10 μM 2-APB was used for stimulation and Ca^{2+} imaging traces are average data from $n = 119–125$ cells/condition. *H,* scatter plots show mean ± S.E. of baseline-subtracted maximal values of Fura-2 ratio units. *I,* 50 μM 2-APB was used for stimulation and Ca^{2+} imaging traces are average data from $n = 114–120$ individual cells/condition. *J,* scatter plots show mean ± S.E. of baseline-subtracted maximal values of Fura-2 ratio units. All traces are averaged from 3 independent experiments. ****, $p < 0.0001$; ***, $p < 0.001$; **, $p < 0.01$; *, $p < 0.05$, Kruskal-Wallis test with Dunn's multiple comparisons to WT parental line.

in an inactive conformation (28). Interestingly, these inhibitory effects on STIM1 puncta formation are abolished in cells overexpressing both STIM1 and ORAI1 (24, 28, 31), suggesting that enhanced STIM1/ORAI1 expression and coupling can overcome 2-APB–mediated inhibition of the STIM1 C terminus. Therefore, we tested whether overexpression of ORAI1 could rescue store-independent Ca^{2+} entry driven by STIM1 in response to 2-APB treatment. Stimulation with 10 μM 2-APB of STIM1/2$^{-/-}$ cells overexpressing STIM2 and ORAI1 showed significantly enhanced Ca^{2+} entry compared with STIM1/2$^{-/-}$ cells overexpressing STIM2 alone (Fig. 4, *A* and *B*). This store-independent Ca^{2+} entry with STIM2/ORAI1 overexpression was even bigger, albeit transient, with 50 μM 2-APB (Fig. 4, *E* and *F*). In contrast, overexpression of STIM1 with ORAI1 marginally enhanced Ca^{2+} entry in response to 10 μM 2-APB compared with STIM1/2$^{-/-}$ cells overexpressing STIM1 alone (Fig. 4, *A* and *B*). Stimulation of STIM1/2$^{-/-}$ cells overexpressing STIM1/ORAI1 with 50 μM 2-APB significantly enhanced Ca^{2+} entry compared with cells overexpressing STIM1 alone, although the magnitude of this effect was drastically less than with STIM2/ORAI1 expression (Fig. 4, *E* and *F*).

Stimulation of STIM1/2$^{-/-}$ cells overexpressing STIM2/ORAI1 with 10 μM 2-APB further enhanced the size of preclustered STIM2 puncta (Fig. 4, *C* and *D*), whereas 2-APB stimulation did not induce puncta formation in STIM1/ORAI1 overexpressing cells (Fig. 4*G*). Taken together, these results suggest that low and high concentrations of 2-APB induce store-independent Ca^{2+} entry through STIM2. Moderate 2-APB–mediated activation of STIM1 is observed only in cells overexpressing STIM1 and ORAI1, and stimulated with high concentrations of 2-APB (50 μM; Fig. 4, *E* and *F*), a finding in agreement with previous reports (24).

Low concentrations of 2-APB potentiate SOCE exclusively through STIM2

We next examined the effects of 2-APB on the potentiation and inhibition of SOCE activated through agonist stimulation. For reasons that will become clear below, we used 100 μM carbachol with 2 mM extracellular Ca^{2+} or 150 μM ATP with 10 mM extracellular Ca^{2+} for HEK293 cells and 300 μM ATP with 10 mM extracellular Ca^{2+} for HCT116 cells. Stimulation with carbachol followed by re-addition of Ca^{2+} to the extracellular

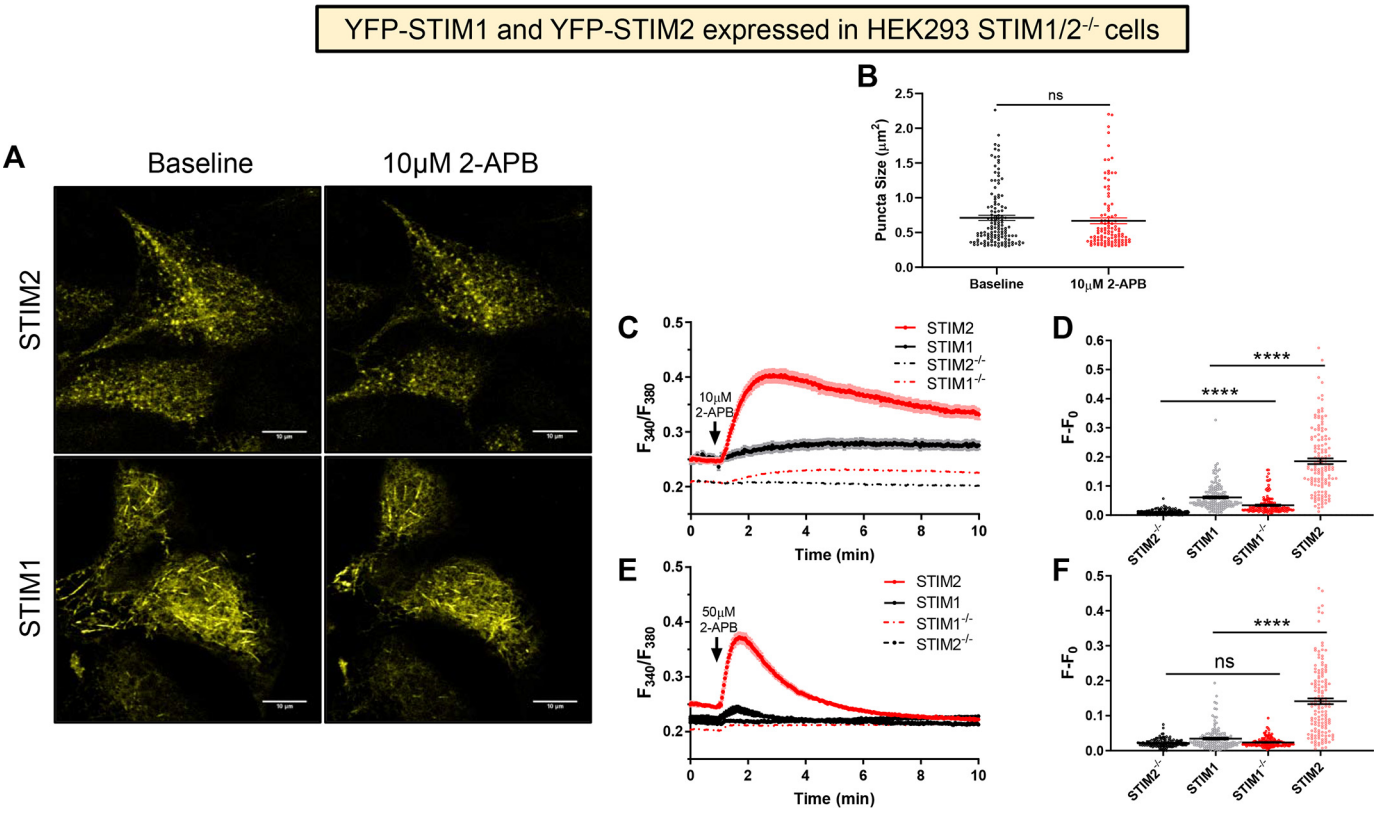

Figure 3. STIM2 is sufficient to rescue store-independent Ca^{2+} entry. *A,* representative confocal images of HEK293 STIM1/2$^{-/-}$ cells expressing either YFP-STIM2 or YFP-STIM1 at baseline and after stimulation with 10 μM 2-APB for 5 min. *B,* quantification of average STIM2 puncta size at baseline and after 10 μM 2-APB stimulation. *C,* HEK293 STIM1/2$^{-/-}$ cells overexpressing YFP-STIM2 (*STIM2*) or YFP-STIM1 (*STIM1*) and stimulated with 10 μM 2-APB in the presence of 2 mM Ca^{2+}. *Dotted traces* represent 10 μM 2-APB-induced Ca^{2+} entry in HEK293 STIM1$^{-/-}$ cells (STIM1$^{-/-}$) or HEK293 STIM2$^{-/-}$ cells (STIM2$^{-/-}$). Ca^{2+} imaging traces are average data from n = 100–118 transfected cells/condition from 3 independent experiments. *D,* scatter plots show mean ± S.E. of baseline-subtracted maximal values of Fura-2 ratio units. *E,* same experimental conditions as in *C,* but with 50 μM 2-APB stimulation. Ca^{2+} imaging traces are average data from n = 99–125 transfected cells/condition from 3 independent experiments. *F,* scatter plots show mean ± S.E. of baseline-subtracted maximal values of Fura-2 ratio units. ****, $p < 0.0001$; *, $p < 0.05$, nonparametric Mann-Whitney test.

medium induced SOCE in WT HEK293 cells. Although HEK293 STIM2$^{-/-}$ cells showed only partial inhibition of SOCE, minimal SOCE was detected in STIM1$^{-/-}$, and essentially no SOCE was observed in STIM1/2$^{-/-}$ cells (Fig. 5*A*). The same protocol using stimulation with ATP showed marginal Ca^{2+} entry in all three knockout cell lines, STIM1$^{-/-}$, STIM2$^{-/-}$, and STIM1/2$^{-/-}$ (Fig. 5*B*), suggesting that ATP is a weak agonist that relies on both STIM1 and STIM2 for SOCE activation. Indeed, 10 mM external Ca^{2+} was used to enhance the driving force and detect a Ca^{2+} signal in WT HEK293 cells. In all conditions, however, subsequent addition of 10 μM 2-APB consistently induced rapid potentiation of SOCE in STIM1$^{-/-}$ cells, whereas no potentiation was observed in STIM2$^{-/-}$ or STIM1/2$^{-/-}$ cells (Fig. 5, *A* and *B*). SOCE was inhibited by the sequential addition of 50 μM 2-APB in all cell lines (Fig. 5, *A* and *B*). WT HEK293 cells showed marginal potentiation with 10 μM 2-APB when SOCE was stimulated with carbachol (Fig. 5*A*), likely because carbachol causes maximal depletion of ER stores and maximal activation of SOCE compared with ATP (Fig. 5*B*). Similar results were observed with ATP in HCT116 cells. Supramaximal ATP concentrations (300 μM with 10 mM Ca^{2+} extracellular; 150 μM ATP did not yield consistent SOCE activation) activated moderate SOCE in WT HCT116 cells, with marginal SOCE detected in STIM1$^{-/-}$ and STIM2$^{-/-}$ cells (Fig. 5*C*). Addition of 10 μM 2-APB potentiated SOCE in WT HCT116 and STIM1$^{-/-}$ cells, but not in STIM2$^{-/-}$ cells. This potentiation was rapidly inhibited following addition of 50 μM 2-APB (Fig. 5*C*). Despite repeated attempts with various protocols, HCT116 cell lines did not respond to carbachol stimulation.

Flexibility of the STIM2 C terminus is critical to 2-APB selectivity

Under conditions of high ER Ca^{2+} concentrations, the C terminus of STIM1 and STIM2 are maintained in an inactive and clamped confirmation characterized by strong molecular interactions between the CC1 and CC3 domains, which shield SOAR domains from ORAI1 (14, 18, 36–39). Depletion of ER stores and loss of Ca^{2+} binding to the luminal EF-hand domains of STIM1 and STIM2 triggers rearrangement of the N and C terminus, opening the CC1/CC3 clamp, and exposing either SOAR1 or SOAR2 for gating and activation of ORAI1 channels (2, 4, 6, 37, 38, 40–42). Accordingly, 2-APB–induced store-independent Ca^{2+} entry is mediated through proper interaction and gating of SOAR2 with ORAI1 channels as the dominant-negative splice variant STIM2.1, containing an 8 amino acid insertion within SOAR2 (43, 44), demonstrated no increase in cytosolic Ca^{2+} concentrations in response to 10 μM 2-APB (Fig. 6, *A* and *B*). In conjunction with the SOAR domains (Fig. 6*C*), studies have described key residues within the C-terminal CC1

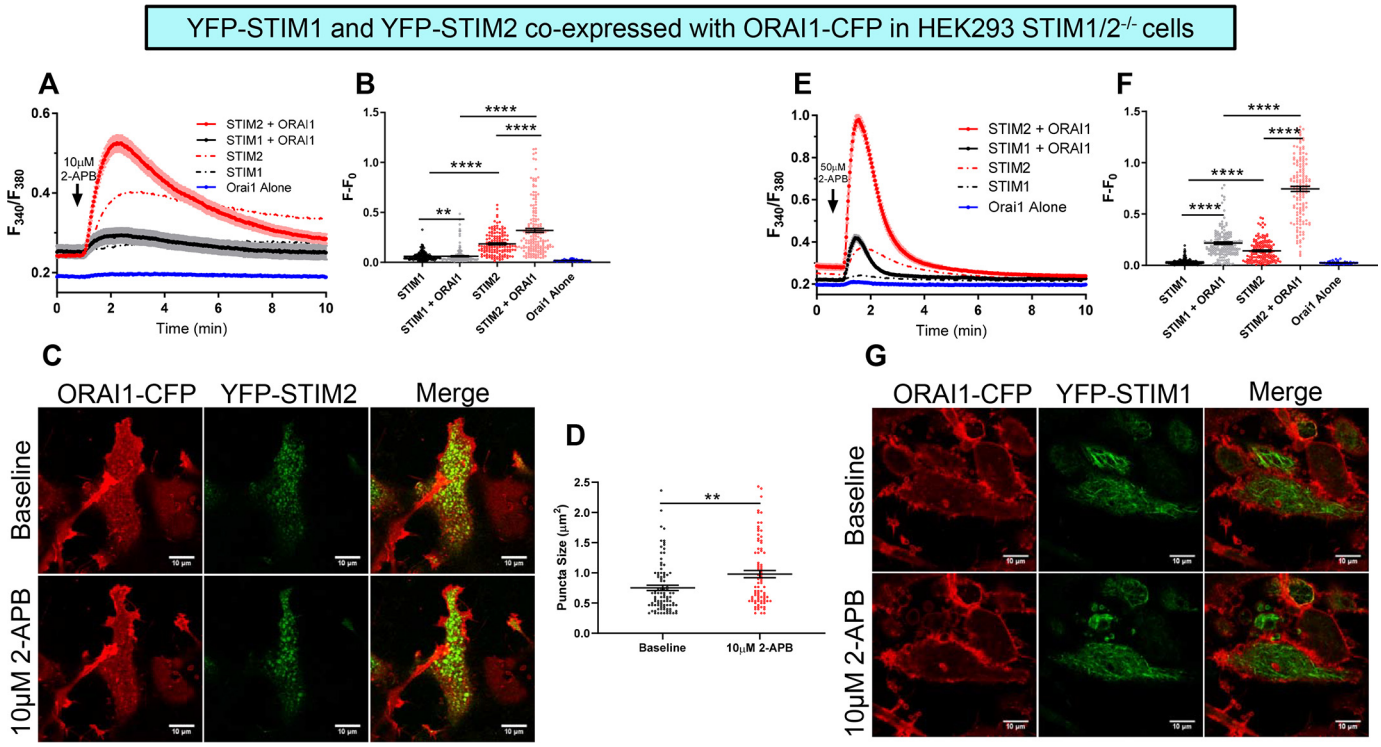

Figure 4. ORAI1 overexpression enhances STIM2, but not STIM1, mediated store-independent Ca^{2+} entry. *A,* HEK293 STIM1/2$^{-/-}$ cells overexpressing ORAI1-CFP and YFP-STIM2 (STIM2 + ORAI1) or ORAI1-CFP and YFP-STIM1 (STIM1 + ORAI1) and stimulated with 10 μM 2-APB in the presence of 2 mM Ca^{2+}. *Dotted traces* represent addition of 10 μM 2-APB to cells overexpressing either STIM1 (*STIM1*) or STIM2 (*STIM2*) alone. Ca^{2+} imaging traces are average data from $n = 165$–176 transfected cells/condition from 3 independent experiments. *B,* scatter plots show mean ± S.E. of baseline-subtracted maximal values of Fura-2 ratio units. *E,* same experimental conditions as in *A,* but with 50 μM 2-APB stimulation. Ca^{2+} imaging traces are average data from $n = 151$–172 transfected cells/condition from 3 independent experiments. *F,* scatter plots show mean ± S.E. of baseline-subtracted maximal values of Fura-2 ratio units. ****, $p < 0.0001$; **, $p < 0.01$; *, $p < 0.05$, nonparametric Mann-Whitney test. *C,* representative confocal images of HEK293 STIM1/2$^{-/-}$ cells overexpressing ORAI1-CFP and YFP-STIM2 at baseline and after stimulation with 10 μM 2-APB for 5 min. *D,* quantification of average STIM2 puncta size in STIM2 + ORAI1 expressing cells (from *C*) at baseline and after 10 μM 2-APB stimulation, nonparametric Mann-Whitney test. *G,* representative confocal images of HEK293 STIM1/2$^{-/-}$ cells overexpressing ORAI1-CFP and YFP-STIM1 at baseline and after stimulation with 10 μM 2-APB for 5 min.

and CC3 domains that contribute to the induction of the active conformation of STIM1 and STIM2 (37, 40). Mutation of residues located within the ORAI1 activating small fragment (OASF1 (37, 40), Fig. 6*C*) region of STIM1 have been identified to either stabilize (R426L) or disrupt (L251S) CC1/CC3 interactions (Fig. 6*C*). Comparison of corresponding mutations in STIM2 that stabilize (R517L) or disrupt (L342S/L507S/L514S, CCmt) CC1/CC3 interactions suggest that the OASF region of STIM2 (OASF2) adopts a weaker CC1/CC3 interaction generating a more flexible conformation of OASF2 compared with OASF1 (19). Utilizing intramolecular FRET-based OASF1 and OASF2 sensors expressed in HEK293 STIM1/2$^{-/-}$ cells, we confirm previous findings of significantly reduced intramolecular FRET signal of the OASF2 region of STIM2 compared with OASF1 of STIM1 (Fig. 6*D*). We further show that OASF1 and OASF2 FRET sensors with mutations predicted to stabilize or disrupt CC1/CC3 interactions behave as expected. The OASF1-L251S mutant predicted to disrupt STIM1 C-terminal interactions displayed significantly reduced intramolecular FRET signal compared with OASF2 (Fig. 6*E*). Conversely, the stabilizing mutant OASF1-R426L displayed a FRET signal comparable with OASF1. Importantly, the triple L342S/L507S/L514S (CCmt) OASF2 mutant displayed significantly decreased FRET signal compared with OASF2 (Fig. 6*E*), suggesting even further flexibility of this mutant. The stabilized OASF2-R517L mutant demonstrated significantly higher FRET signal than OASF2, which was still substantially less than OASF1 (Fig. 6*E*). We next tested the ability of 10 μM 2-APB to induce changes in intramolecular FRET of OASF1 and OASF2 constructs and observed marginal FRET changes with all different OASF variants (Fig. 6, *F* and *G*; see *H* and *I* for zoom-in normalized FRET), suggesting that any rearrangements of C-terminal STIM caused by 2-APB are likely very subtle. These results are consistent with data from the Romanin group (37) showing that, without overexpression of ORAI1, even high concentrations (75 μM) of 2-APB caused a marginal decrease in OASF1 intramolecular FRET.

We next evaluated the effects of CC1/CC3 stabilization or disruption mutations on 2-APB–mediated Ca^{2+} entry by expressing these mutations within the context of full-length STIM1 and STIM2 proteins in HEK293 STIM1/2$^{-/-}$ cells. Similar to overexpression of STIM2, both the flexible CCmt-STIM2 and stabilized R517L-STIM2 mutants displayed extensive preformed puncta (Fig. 7*A*). Although all STIM2 mutants showed reorganization of baseline puncta in response to the change in shape of cells, 2-APB did not lead to significant enhancement of puncta size (Fig. 7*B*). Stimulation of STIM2-expressing cells with 10 μM 2-APB induced rapid and sustained store-independent Ca^{2+} entry (Fig. 7, *C* and *D*), as shown in Fig. 3, *C* and *D*. Interestingly, the flexible CCmt-STIM2 displayed

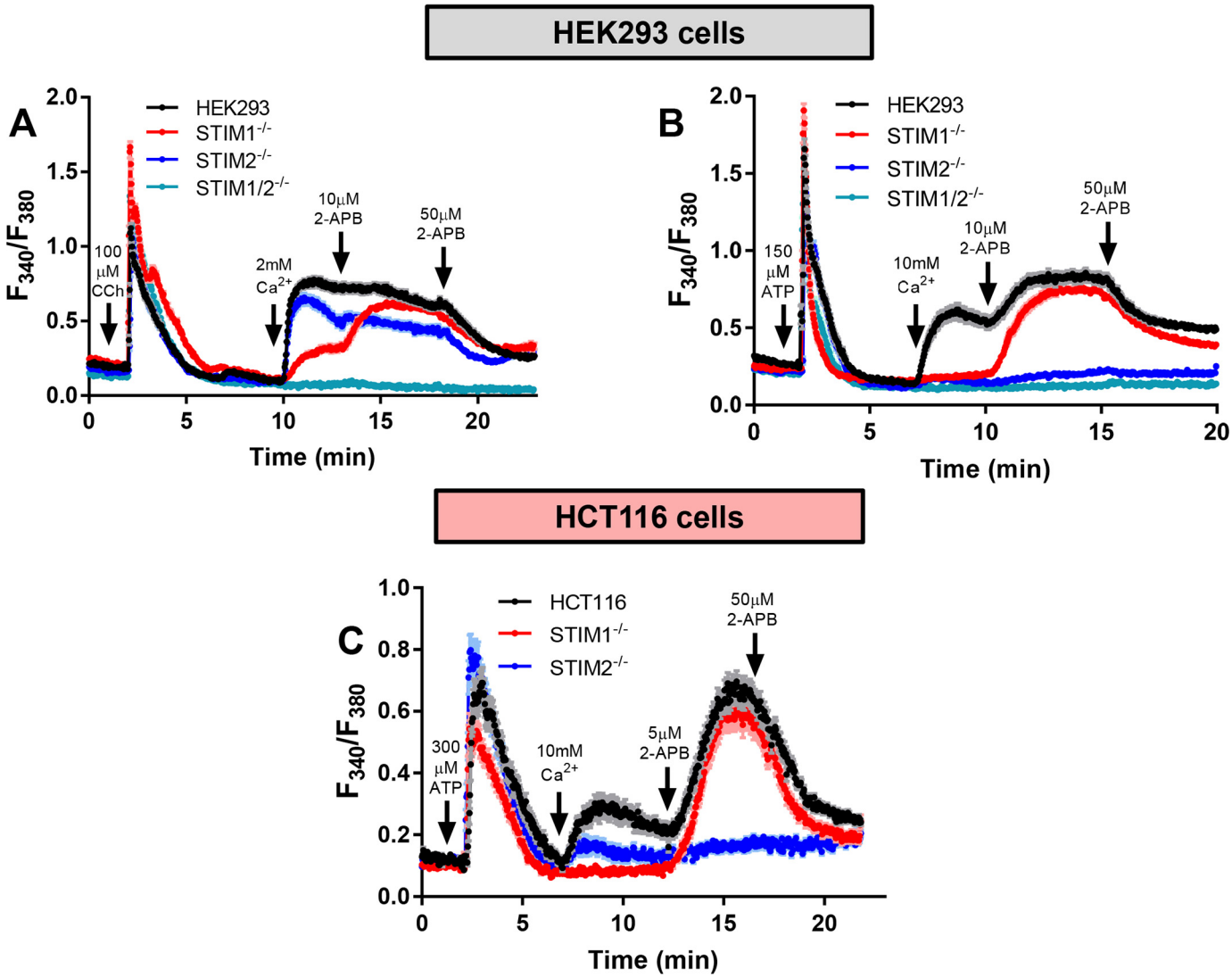

Figure 5. Low concentrations of 2-APB potentiate SOCE through STIM2. *A,* measurement of carbachol-induced SOCE in WT HEK293 and STIM CRISPR cell lines. Cells were stimulated with 100 μM carbachol in a nominally Ca^{2+}-free solution followed by re-introduction of 2 mM Ca^{2+} to the extracellular medium. 10 and 50 μM 2-APB were added in the presence of extracellular Ca^{2+} at the indicated times. Ca^{2+} imaging traces are average data from n = 101–140 cells/condition from 3 independent experiments. *B,* same experimental conditions as in *A,* but with 150 μM ATP in a nominally Ca^{2+}-free solution, followed by re-introduction of 10 mM Ca^{2+} (instead of 2 mM) to the extracellular medium. 10 mM was used to enhance the driving force and reveal responses to ATP, which were undetectable in 2 mM external Ca^{2+}. Ca^{2+} imaging traces are average data from n = 116–135 cells/condition from 3 independent experiments. *C,* measurement of ATP-induced SOCE in WT HCT116 and STIM CRISPR cell lines. Cells were stimulated with 300 μM ATP in a nominally Ca^{2+}-free solution, followed by re-introduction of 10 mM Ca^{2+} to the extracellular medium. The use of 150 μM ATP in HCT116 cells generated small and inconsistent SOCE. 10 and 50 μM 2-APB were added in the presence of extracellular Ca^{2+} at the indicated times. Ca^{2+} imaging traces are average data from n = 60–100 cells/condition from 3 independent experiments.

substantially increased Ca^{2+} entry compared with STIM2, whereas the stabilized R517L-STIM2 supported Ca^{2+} entry that was slightly reduced compared with STIM2 (Fig. 7, *C* and *D*). Similar results were obtained when STIM2 mutants were stimulated with 50 μM 2-APB (Fig. 7, *E* and *F*). However, the stabilized R517L-STIM2 mutant displayed nearly identical Ca^{2+} entry compared with STIM2 (Fig. 7, *E* and *F*).

STIM1 and the stabilized R426L-STIM1 mutant expressed in STIM1/2$^{-/-}$ cells displayed tubular localization throughout the cell, whereas the flexible L251S-STIM1 had extensively preformed puncta (Fig. 8*A*). Stimulation of STIM1 with 10 μM 2-APB induced minimal store-independent Ca^{2+} entry, which was completely abolished in the stabilized R426L-STIM1 mutant (Fig. 8, *C* and *D*). The flexible L251S-STIM1 mutant showed preformed puncta and constitutive Ca^{2+} activity (Fig. 8*B*) as previously reported (37). Unexpectedly, however, it supported minimal Ca^{2+} entry in response to 10 μM 2-APB that was comparable with STIM1 (Fig. 8, *C* and *D*). In response to 50 μM 2-APB, STIM1 and the flexible L251S-STIM1 mutants showed similar patterns of small initial Ca^{2+} entry to those seen on stimulation with 10 μM 2-APB, whereas the stabilized R426L-STIM1 showed essentially no response (Fig. 8, *E* and *F*). Furthermore, basal activity of the L251S-STIM1 mutant was subsequently inhibited by 50 μM 2-APB (Fig. 8*E*). Our results thus far suggest that whereas the increased flexibility of the STIM2 C terminus plays a key role in driving Ca^{2+} entry in response to 2-APB and weak agonists, enhanced C-terminal flexibility alone cannot rescue the activation of STIM1 by 2-APB.

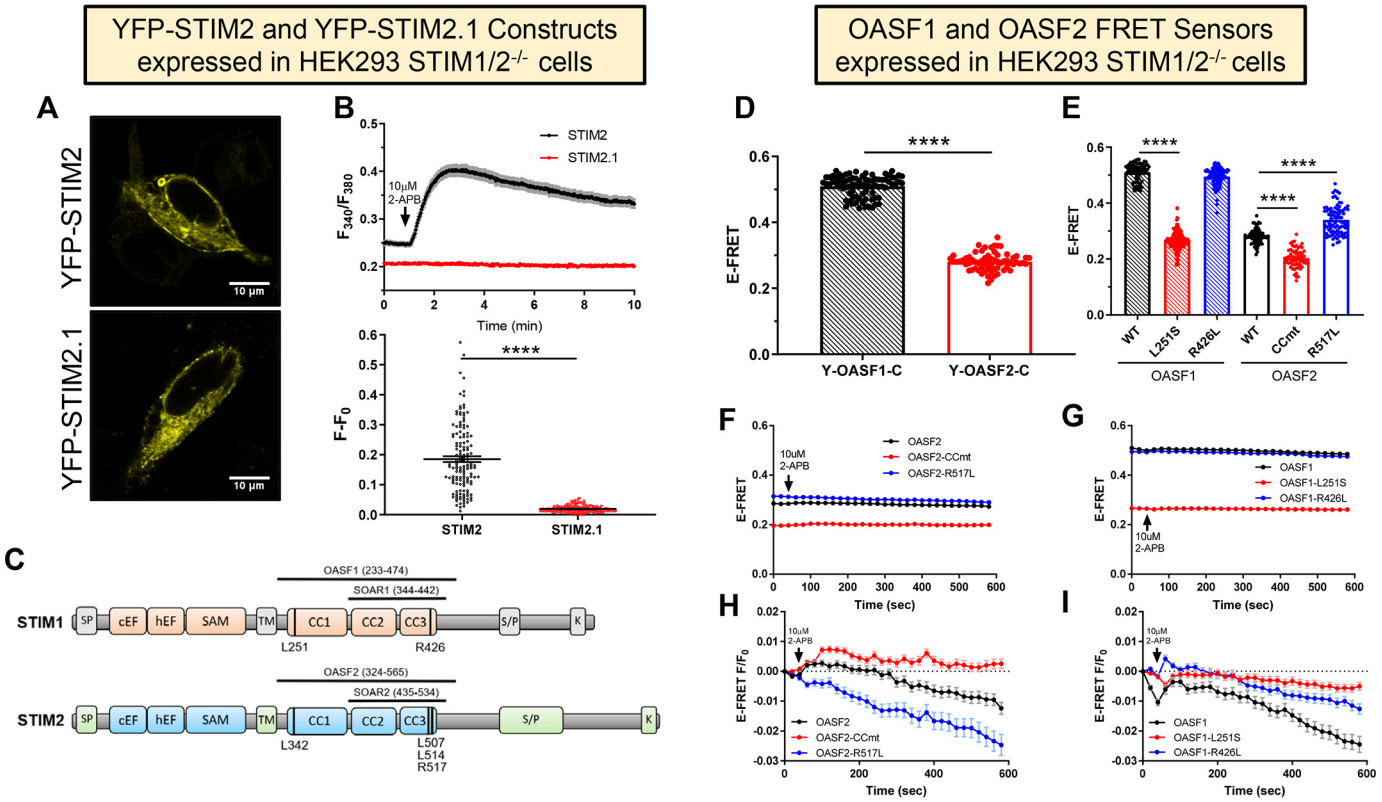

Figure 6. Differential CC1/CC3 interactions contribute to increased flexibility of the STIM2 C terminus. *A,* representative confocal images of HEK293 STIM1/2$^{-/-}$ cells expressing either YFP-STIM2 or YFP-STIM2.1. *B,* HEK293 STIM1/2$^{-/-}$ cells overexpressing YFP-STIM2 or YFP-STIM2.1 and stimulated with 10 μM 2-APB in the presence of 2 mM Ca^{2+}. Ca^{2+} imaging traces are average data from $n = 122–159$ transfected cells/condition from 3 independent experiments. Scatter plots show mean ± S.E. of baseline-subtracted maximal values of Fura-2 ratio units. ****, $p < 0.0001$, nonparametric Mann-Whitney test. *C,* diagram of STIM1 and STIM2 structure showing CC1 and CC3 stabilization/disruption mutations. *D,* OASF FRET sensors for STIM1, YFP-OASF1-CFP (Y-OASF1-C), and for STIM2, YFP-OASF2-CFP (Y-OASF2-C), were expressed in HEK293 STIM1/2$^{-/-}$ cells and a baseline E-FRET signal was measured from Y-OASF1-C and Y-OASF2-C. ****, $p < 0.0001$, nonparametric Mann-Whitney test. *E,* scatter plots demonstrating the distribution of intramolecular FRET signal from STIM1/2$^{-/-}$ cells overexpressing YFP-OASF1-CFP or YFP-OASF2-CFP (WT) or their stabilization and disruption mutants. ****, $p < 0.0001$; ***, $p < 0.001$, mutants were compared with WT constructs using nonparametric Mann-Whitney tests. *F* and *G,* intramolecular FRET in HEK293 STIM1/2$^{-/-}$ cells expressing either OASF2 (*F*) or OASF1 (*G*) WT and mutant variants under basal conditions and after addition of 10 μM 2-APB. *H* and *I,* zoomed-in and normalized FRET data from *F* and *G,* respectively.

Recent reports have demonstrated that STIM2 remodels the STIM1 C terminus under conditions of high ER Ca^{2+} concentrations to allow interactions with ORAI1 under low stimulus intensities (18, 19). We examined this effect by co-expression of STIM1 and STIM2 in STIM1/2$^{-/-}$ cells. Interestingly, the expression of both STIM1 and STIM2 led to significant constitutive activity by comparison to either STIM expressed alone (Fig. 8*G*). Stimulation with either 10 μM (Fig. 8, *H* and *I*) or 50 μM (Fig. 8, *J* and *K*) 2-APB activated significant Ca^{2+} entry in cells expressing STIM2 or co-expressing both STIM proteins but not in cell expressing STIM1 alone.

Coordination between STIM2 N and C termini is required for 2-APB sensitivity

We next determined the contribution of the STIM2 N terminus in mediating store-independent Ca^{2+} entry by constructing two chimeric STIM constructs: a chimera of STIM1 N terminus with the STIM2 TM and C terminus (S1N-S2C) and another of STIM2 N terminus with the STIM1 TM and C terminus (S2N-S1C; Fig. 9*A*). Interestingly, expression of the S1N-S2C chimera in HEK293 STIM1/2$^{-/-}$ cells showed preformed puncta throughout the cell (Fig. 9*B*, *top*), whereas expression of the S2N-S1C chimera displayed diffuse ER localization similar to STIM1 (Fig. 9*B*, *bottom*), further confirming that STIM2 preformed puncta are driven by its C terminus and not by the enhanced sensitivity of its N terminus to store depletion (6). Each STIM chimera was overexpressed in STIM1/2$^{-/-}$ cells to measure SOCE in response to store depletion with thapsigargin (Fig. 9, *C* and *D*). Stimulation of S1N-S2C– expressing cells displayed a similar release of ER Ca^{2+} compared with S2N-S1C– expressing cells and nontransfected STIM1/2$^{-/-}$ cells. However, S2N-S1C overexpression resulted in increased constitutive activity (Fig. 9, *F* and *G*). SOCE was significantly rescued with expression of either S1N-S2C or S2N-S1C chimeras. However, S2N-S1C expression supported bigger SOCE (Fig. 9, *C* and *D*), likely the result of its enhanced constitutive activity. Interestingly, addition of 50 μM 2-APB strongly inhibited SOCE mediated by the S2N-S1C chimera with less inhibitory effect on SOCE supported by the S1N-S2C chimera (Fig. 9, *C–E*), suggesting the STIM2 C terminus protects against 2-APB–mediated inhibition. These findings are consistent with the reported constitutive activity of a similar STIM1 chimera containing the EF-SAM domain of STIM2 co-expressed with ORAI1 (45). We then determined the ability of the STIM chimeras to mediate store-independent Ca^{2+} entry in response to 2-APB stimulation when expressed in STIM1/2$^{-/-}$ cells. As expected, overexpression of STIM2 supported a sustained

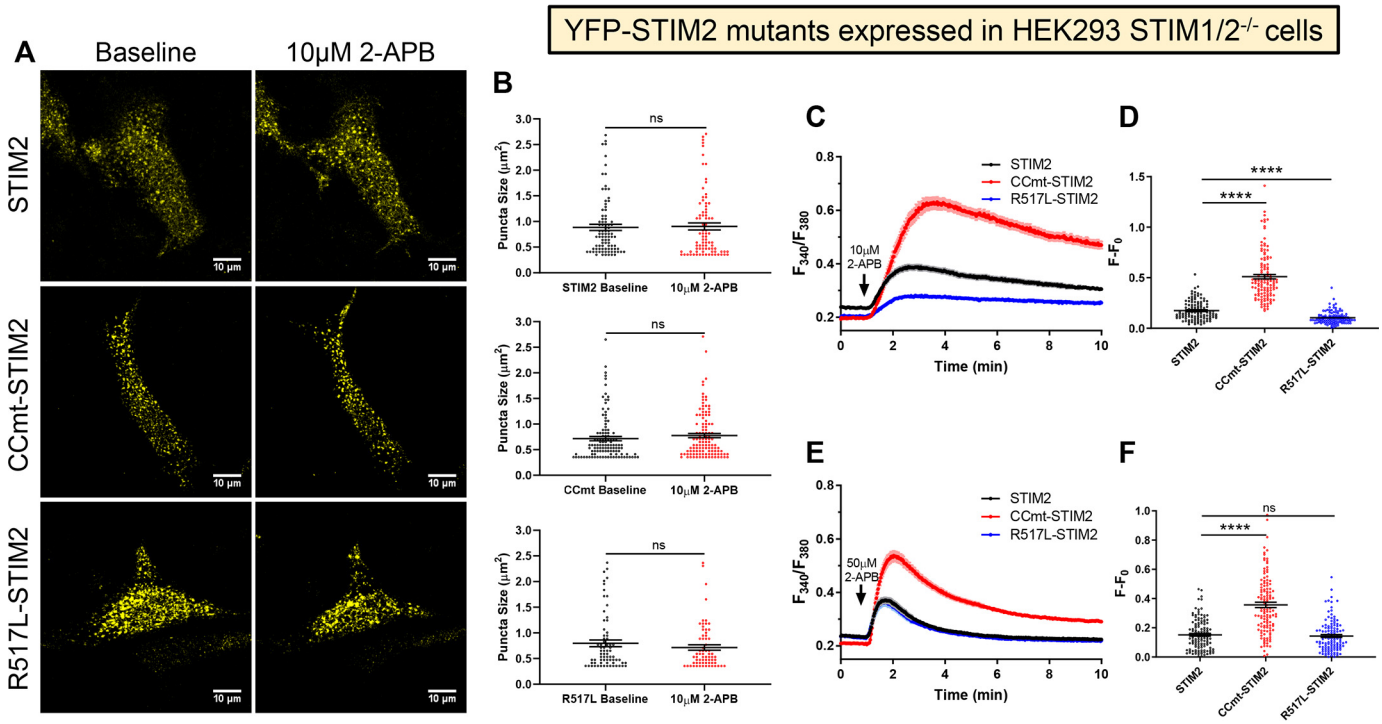

Figure 7. Flexibility of the STIM2 C terminus contributes to 2-APB selectivity. *A,* representative confocal images of HEK293 STIM1/2$^{-/-}$ cells expressing YFP-STIM2 or YFP-tagged mutants, including the relaxed CCmt-STIM2 (L342S/L507S/L514S) mutant, or the stabilized R517L-STIM2 mutant at baseline and after stimulation with 10 μM 2-APB. *B,* quantification of average puncta size in STIM2, CCmt-STIM2, and R517L-STIM2 mutants at baseline and after 10 μM 2-APB stimulation. *C,* HEK293 STIM1/2$^{-/-}$ cells overexpressing YFP-tagged versions of STIM2, CCmt-STIM2, or R517L-STIM2, and stimulated with 10 μM 2-APB in the presence of 2 mM Ca^{2+}. Ca^{2+} imaging traces are average data from $n = 113–120$ transfected cells/condition from 3 independent experiments. *D,* scatter plots show mean ± S.E. of baseline-subtracted maximal values of Fura-2 ratio units. ****, $p < 0.0001$, Kruskal-Wallis test with Dunn's multiple comparisons of STIM2 mutants to WT STIM2. *E,* same as in *C* but stimulation with 50 μM 2-APB in the presence of 2 mM Ca^{2+}. Ca^{2+} imaging traces are average data from $n = 119–127$ transfected cells/condition from 3 independent experiments. *F,* scatter plots show mean ± S.E. of baseline-subtracted maximal values of Fura-2 ratio units. ****, $p < 0.0001$, Kruskal-Wallis test with Dunn's multiple comparisons of STIM2 mutants to WT STIM2.

Ca^{2+} entry in response to 10 μM 2-APB, whereas STIM1 overexpression mediated marginal Ca^{2+} entry under the same conditions (Fig. 9, *H* and *I*). Unexpectedly, both S1N-S2C and S2N-S1C chimeras mediated minimal Ca^{2+} entry comparable with STIM1 in response to 10 μM 2-APB (Fig. 9, *H* and *I*). Similar results were observed when cells were stimulated with 50 μM 2-APB with each STIM chimera displaying minimal store-independent Ca^{2+} entry (Fig. 9, *J* and *K*). These results suggest that both the high sensitivity of the STIM2 N terminus and the communication with the flexible conformation of its C terminus are key determinants for activation of store-independent Ca^{2+} entry in response to 2-APB, and likely in response to weak agonists or low concentrations of strong agonists.

Discussion

Recent studies have defined unique functions for STIM2 in regulating cytosolic Ca^{2+} signals under conditions of minimal ER Ca^{2+} depletion (18, 19). Upon stimulation with low concentrations of agonist that minimally deplete intracellular stores, STIM2 has been demonstrated to recruit STIM1 into ER–PM junctions to interact with ORAI1 channels and drive SOCE under conditions where STIM1 would normally be unable to oligomerize and form puncta (18). Mechanistically, the increased flexibility of the STIM2 C-terminal OASF2 region along with higher phosphatidylinositol 4,5-biphosphate binding affinity of the C-terminal polybasic domain are suggested to account for constitutive activation and preformed puncta of STIM2 under resting conditions (19, 46). The flexibility of OASF2 triggers remodeling of the STIM1 C terminus for interaction and gating of ORAI1 under high ER Ca^{2+} concentrations, possibly through heteromeric interactions between STIM1 and STIM2 (18). Previous studies investigated the effects of high concentrations of 2-APB on STIM and ORAI using overexpression and showed that 2-APB induces avid binding of cytosolic C termini of both STIM1 and STIM2 to ORAI1 causing increased channel activity (24). Functional binding of expressed STIM1 C terminus to ORAI1 also occurred in DT40 chicken B cells lacking endogenous STIM1 and STIM2, indicating that C-terminal fragments work independently of native STIMs and that STIM C terminus is critical for 2-APB action (24). Here we show that under native levels of expression, both the N terminus and C terminus of STIM2 are necessary and sufficient for enhanced STIM2 sensitivity, suggesting that weak agonists or low concentrations of strong agonists use STIM2 to enhance the diversity of physiological Ca^{2+} signals. Through the use of multiple CRISPR/Cas9 cell lines with STIM1 and STIM2 knocked out individually or in combination, we conclude that 2-APB–activated store-independent Ca^{2+} entry is mediated exclusively by endogenous STIM2. This store-independent entry was significantly enhanced with STIM2 overexpression in HEK293 STIM1/2$^{-/-}$ cells and augmented further when STIM2 was expressed in combination with ORAI1. Importantly, STIM2-dependent 2-APB–activated

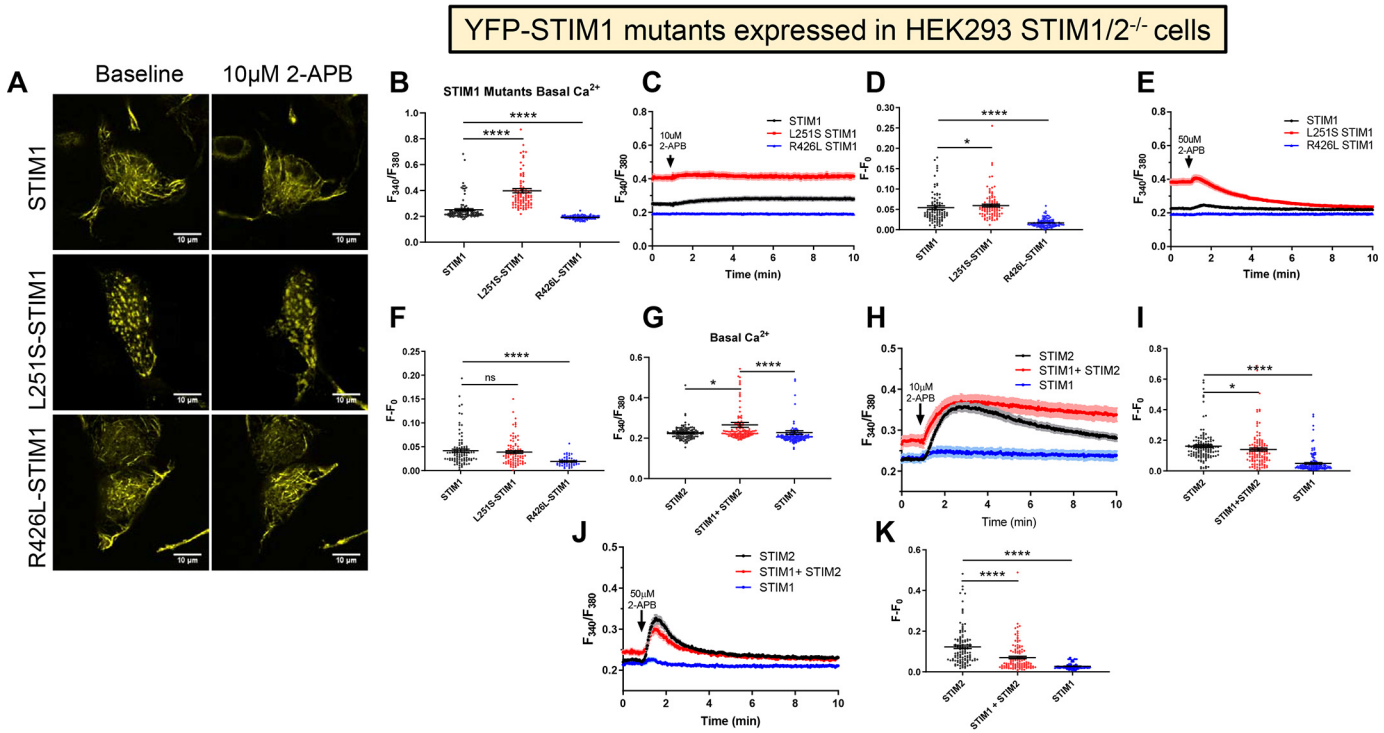

Figure 8. Increased flexibility of the STIM1 C terminus is not sufficient to recapitulate store-independent Ca^{2+} entry. *A,* representative confocal images of HEK293 STIM1/2$^{-/-}$ cells expressing YFP-tagged versions of STIM1, the relaxed L251S-STIM1 mutant, or the stabilized R426L-STIM1 mutant at baseline and after stimulation with 10 μM 2-APB. *B,* quantification of basal Ca^{2+} levels in cells expressing STIM1, L251S-STIM1, or R426L-STIM1 mutants prior to 2-APB stimulation. *C,* HEK293 STIM1/2$^{-/-}$ cells overexpressing YFP-tagged versions of STIM1, L251S-STIM1, or R426L-STIM1 and stimulated with 10 μM 2-APB in the presence of 2 mM Ca^{2+}. Ca^{2+} imaging traces are average data from $n = 95–100$ transfected cells/condition from 3 independent experiments. *D,* scatter plots show mean ± S.E. of baseline-subtracted maximal values of Fura-2 ratio units. *E,* same experimental conditions as in *C,* but with 50 μM 2-APB stimulation. Ca^{2+} imaging traces are average data from $n = 50–99$ transfected cells/condition from 3 independent experiments. *F,* scatter plots show mean ± S.E. of baseline-subtracted maximal values of Fura-2 ratio units. ****, $p < 0.0001$, Kruskal-Wallis test with Dunn's multiple comparisons of STIM1 mutants to WT STIM1. *G,* quantification of basal Ca^{2+} levels in cells expressing STIM1, STIM2, or STIM1 + STIM2 prior to 2-APB stimulation. *H,* same as in *C,* but with overexpression of YFP-tagged versions of STIM2, STIM1, or STIM1 + STIM2 and stimulated with 10 μM 2-APB in the presence of 2 mM Ca^{2+}. *I,* scatter plots show mean ± S.E. of baseline-subtracted maximal values of Fura-2 ratio units. *J,* same experimental conditions as in *E,* but with overexpression of YFP-tagged versions of STIM2, STIM1, or STIM1 + STIM2 and stimulated with 50 μM 2-APB in the presence of 2 mM Ca^{2+}. *K,* scatter plots show mean ± S.E. of baseline-subtracted maximal values of Fura-2 ratio units.

Ca^{2+} entry could not be rescued with overexpression of STIM1 alone or with STIM1 and ORAI1 overexpression. Only high concentrations of 2-APB (50 μM) could induce a moderate level of store-independent Ca^{2+} entry in STIM1/ORAI1 overexpressing cells that was ~⅓ of that observed in cells overexpressing STIM2/ORAI1 and stimulated by the same concentration of 2-APB. By testing full-length STIM1 and STIM2 variants with mutations predicted to stabilize or disrupt CC1/CC3 interactions, we determined that increased flexibility of the STIM2 C terminus plays a significant role in response to 2-APB–mediated Ca^{2+} entry. Introduction of a stabilization mutation (R517L) shown to restrict STIM2 C-terminal flexibility and strengthen its CC1/CC3 interactions slightly reduced Ca^{2+} entry in response to 10 μM 2-APB compared with STIM2. Importantly, introduction of a mutation into the C terminus of STIM1 (L251S) making it more flexible caused preformed STIM1 puncta and induced constitutive Ca^{2+} entry, but could not support store-independent Ca^{2+} entry in response to low or high concentrations of 2-APB. These data suggest that whereas increased flexibility of the STIM2 C terminus is a critical factor in the induction of store-independent Ca^{2+} entry, it is not sufficient.

In addition to differences in CC1/CC3 interactions and differences in key residues, phenylalanine (Phe-394) in SOAR1 is a leucine in SOAR2 and glycine (Gly-379) in SOAR1 is a glutamate in SOAR2, functional differences within the STIM2 N terminus also distinguish its activity from STIM1. Substitution of three amino acids within the N-terminal EF-hand domain of STIM2 confer reduced Ca^{2+} binding affinity, lowering the threshold of STIM2 to induce an active conformation in response to minor reductions in ER Ca^{2+} concentrations (11). Although mutation of these residues in the STIM1 EF-hand to mimic STIM2 increases the Ca^{2+} sensitivity of STIM1, conversion of the STIM2 EF-hand into the corresponding STIM1 residues failed to mimic the activation kinetics of STIM1 (11). Our chimeric STIM constructs demonstrated that substitution of the entirety of STIM1 N terminus with that of STIM2 failed to activate store-independent Ca^{2+} entry in response to 2-APB stimulation. Similarly, replacement of the STIM2 N terminus with that of STIM1 reduced the response to 2-APB to levels similar to STIM1. These data suggest that enhanced sensitivity of the STIM2 N terminus in concert with the increased flexibility of its C terminus are responsible for the unique store-independent activation of STIM2.

Conventional models of SOCE and the regulation of cytosolic Ca^{2+} signals have long placed STIM1 as the primary activator of ORAI channels in response to substantial ER depletion, whereas STIM2 is believed to act as a homeostatic

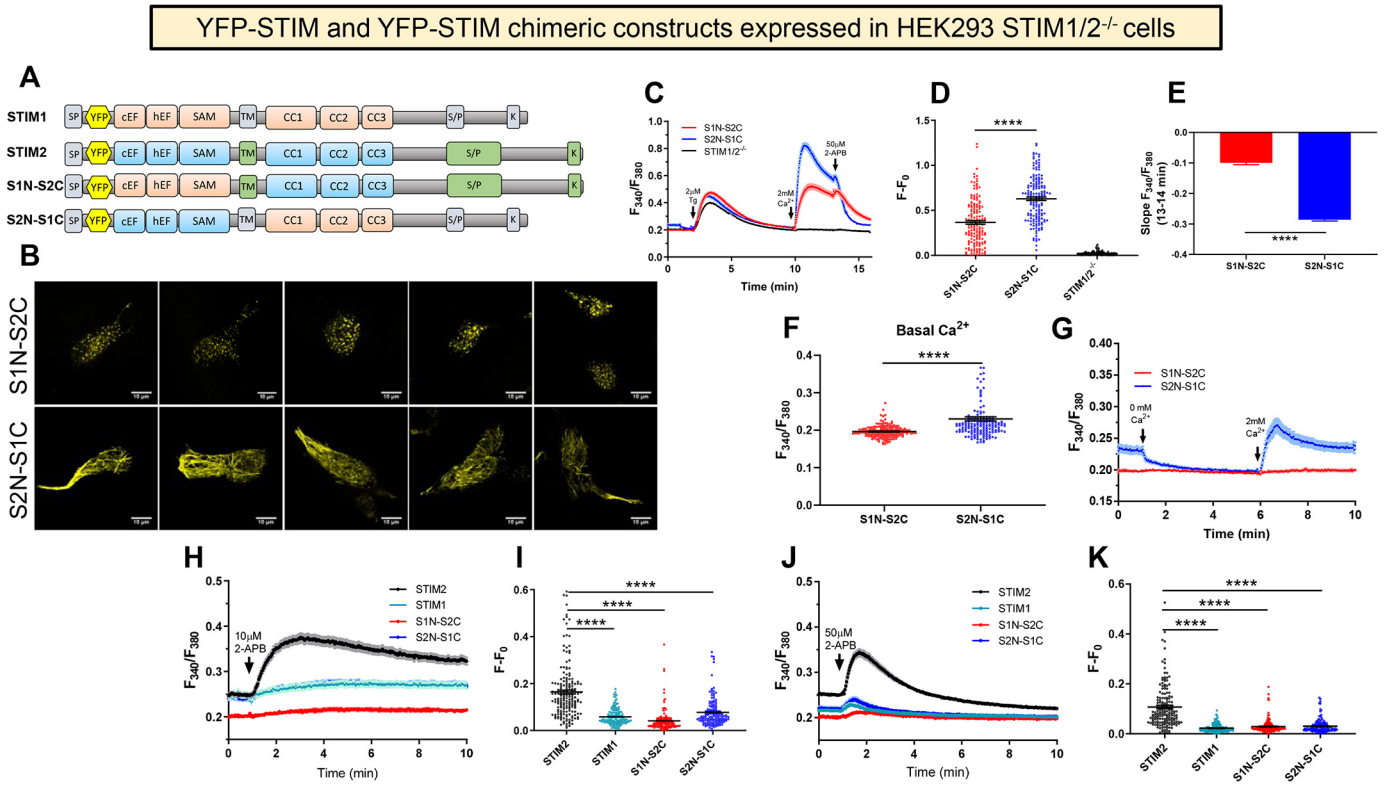

Figure 9. Coordination between STIM2 N and C terminus underlies 2-APB sensitivity. *A,* schematic of YFP-STIM1, YFP-STIM2, and STIM chimeric constructs used for Ca^{2+} imaging experiments. *B,* representative confocal images of several HEK293 STIM1/2$^{-/-}$ cells expressing either chimeric YFP-S1N-S2C (*top*) or YFP-S2N-S1C (*bottom*) constructs. *C,* measurement of thapsigargin-activated SOCE in control HEK293 STIM1/2$^{-/-}$ cells or cells overexpressing YFP-S1N-S2C or YFP-S2N-S1C. Cells were stimulated with 2 μM thapsigargin in a nominally Ca^{2+}-free solution, followed by re-introduction of 2 mM Ca^{2+} to the extracellular medium. 50 μM 2-APB was added in the presence of extracellular Ca^{2+} at the indicated time. Ca^{2+} imaging traces are average data from n = 112–151 cells/condition from 3 independent experiments. *D,* peak SOCE was calculated as baseline-subtracted maximal values of Fura-2 ratio units. *E,* quantification of the slope of inhibition Ca^{2+} entry by 50 μM 2-APB in cells expressing YFP-S1N-S2C or YFP-S2N-S1C chimeras. *F,* quantification of basal Ca^{2+} levels in cells expressing YFP-S1N-S2C or YFP-S2N-S1C. *G,* constitutive activity of HEK293 STIM1/2$^{-/-}$ cells overexpressing YFP-tagged versions of either S1N-S2C or S2N-S1C chimeras. Cells were maintained in a nominally Ca^{2+}-free solution for 5 min followed by restoration of 2 mM Ca^{2+} to extracellular milieu to determine basal unregulated activity. Data are average from n = 164–166 cells/condition from 3 independent experiments. *H,* HEK293 STIM1/2$^{-/-}$ cells overexpressing YFP-tagged versions of STIM1, STIM2, S1N-S2C, or S2N-S1C and stimulated with 10 μM 2-APB in the presence of 2 mM Ca^{2+}. Ca^{2+} imaging traces are average data from n = 122–180 transfected cells/condition from 3 independent experiments. *I,* scatter plots show mean ± S.E. of baseline-subtracted maximal values of Fura-2 ratio units. *J,* similar protocol to *H,* but stimulation with 50 μM 2-APB. Ca^{2+} imaging traces are average data from n = 143–191 transfected cells/condition from 3 independent experiments. *K,* scatter plots show mean ± S.E. of baseline-subtracted maximal values of Fura-2 ratio units.

housekeeping sensor that maintains basal Ca^{2+} concentrations (11, 12). Unique structural features of STIM2 N and C termini dampen its interaction with ORAI channels to prevent Ca^{2+} overload as a result of its constitutive activity in ER–PM junctions (6, 11). Our data utilizing multiple STIM knockout cell lines show that depending on the cell type, native STIM2 can play a significant role in sustaining SOCE when ER Ca^{2+} is maximally depleted. Knockout of STIM2 in HEK293 cells resulted in a minor reduction (~16% inhibition) of peak SOCE compared with WT cells, whereas STIM2 knockout in HCT116 drastically reduced SOCE (~56% inhibition) with no obvious compensatory effect on STIM1 protein levels in either cell line. Furthermore, we noted no differences in STIM1 and STIM2 protein expression between HEK293 and HCT116 cell lines. It is tempting to speculate that in HCT116 cells, STIM2 interacts with and remodels the C terminus of STIM1 into an active conformation despite ER Ca^{2+} being significantly depleted. In support of this idea, knockout of STIM1 in HCT116 cells augmented store-independent Ca^{2+} entry in response to low and high concentrations of 2-APB, suggesting that STIM1 and STIM2 might dynamically regulate the function of one another in a cell type-specific manner. Our results in HCT116 cells are in line with recent data in NIH3T3 fibroblasts and αT3 cells where knockout of STIM2 resulted in a 90% reduction in SOCE (47). In addition to these cell types, a multitude of studies have identified STIM2 as the predominant STIM isoform regulating SOCE in primary neurons (48–50). STIM2-mediated Ca^{2+} entry plays a critical role in maintaining mushroom dendritic spine development *in vitro* and *in vivo* as well as regulating neuronal apoptosis in response to environmental stress (48, 50–52). The use of 2-APB and newly characterized 2-APB analogues (53–55) will be critical in understanding the endogenous interactions between STIM1 and STIM2 and how these ER sensors positively and negatively regulate one another in various physiological systems. Our findings elucidating the differential effects of 2-APB on STIM1 and STIM2 offers readily exploitable approaches to understand the endogenous interactions between STIM1 and STIM2 and might lead to drugs that specifically distinguish STIM2-mediated from STIM1-driven (patho)physiological functions.

Experimental procedures

Cell culture and transfection

HEK293 cells were maintained in high glucose (4.5 g/liter) Dulbecco's modified Eagle's medium supplemented with 10% heat-inactivated fetal bovine serum, penicillin (100 units/ml), streptomycin (100 mg/ml), and cultured in a 5% CO_2 incubator at 37 °C. HCT116 cells were maintained in McCoy's 5A medium supplemented with 10% heat-inactivated fetal bovine serum, penicillin (100 units/ml), streptomycin (100 mg/ml), and cultured in the same incubation conditions. Cells were transfected with either a Nucleofector II Device (Amaxa Biosystems) and the Nucleofector Kit V (VCA-1003) following the manufacturer's protocol or with Lipofectamine 2000 (Invitrogen). After transfection, cells were plated onto 25-mm round glass coverslips and incubated for 24 h before use in experiments (56, 57).

DNA constructs

For use in confocal and Ca^{2+} imaging experiments, pEX-CMV-SP-YFP-STIM2(15–746) (Addgene plasmid number 18862) and pEX-SP-YFP-STIM1(23–685) (Addgene plasmid number 18857), were gifts from Tobias Meyer. pECFP-C1-Orai1 and YFP-STIM2.1 were from Donald Gill. STIM1 CC1/CC3 stabilization and disruption mutants (STIM1-L251S and STIM1-R426L) and OASF FRET sensors were gifts from Christoph Romanin. STIM2 CC1/CC3 stabilization and disruption mutants (STIM2-L342S/L507S/L514S-(CCmt) and STIM2-R517L) and OASF2 FRET sensors were gifts from Indu S. Ambudkar. STIM chimeras were cloned using the In-Fusion system (Takara). Briefly, STIM2N-STIM1C was generated by mixing two primers (CFP-R and S2-S1TM F) with pEX-CMV-SP-YFP-STIM1 to generate a vector lacking amino acids 21–213 of STIM1. The STIM2 insert for STIM2N-STIM1C was generated by mixing two primers (Vector-F and S1TM-S2 R) with pEX-CMV-SP-YFP-STIM2. The above vector and insert were combined according to the In-Fusion protocol to generate the final STIM1N-STIM2C. Using the same method as above to generate STIM2N-STIM1C, two primers (CFP-R and S1-S2TM F) were combined with pEX-CMV-SP-YFP-STIM2 to generate a STIM2 vector lacking aa 15–208. This was then mixed with the STIM1 N-terminal fragment (aa 21–213) generated by mixing primers Vector-F with S2TM-S1R with pEX-SP-YFP-STIM1 to generate the STIM1N-STIM2C construct. Primer sequences utilized for cloning of STIM chimeras were as follows: S2-S1TM F, AAGATTTTTTCATGCTGGTGGTGTCTATC; S1TM-S2 R, GCATGAAAAAATCTTTCATCCAGTTATGAG; S1-S2TM F, CAAGGACATCCTCACAATTTCTATAGTAATTGGT; S2TM-S1R, GTGAGGATGTCCTTGAGGTGATTATGGC; CFP-R, TCGTCCATGCCGAGAGTGAT; Vector-F, TCTCGGCATGGACGAGCTGT.

Generation of STIM1, STIM2, and STIM1/2 double knockout cell lines

Guide RNAs with sequences specific for *STIM1* or *STIM2* were designed and inserted into the BsmBI restriction site of the lentiCRISPR v2 vector (Addgene plasmid number 52961). The guide sequences used were the following: STIM1g1, 5′-TGATGAGCTTATCCTCACCA-3′; STIM2g1, 5′-AGATGGTGGAATTGAAGTAG-3′; and STIM2g2, 5′-AGAAGAAGACAGATTTAGTC-3′. HEK293 cells were transfected with the cloned lentiCRISPR v2 vectors using a Nucleofector II Device (Amaxa Biosystems) and HCT116 were transfected using Lipofectamine 2000 (Invitrogen). 48 h after transfection, HEK293 and HCT116 cells were cultured with their respective media containing puromycin (2 μg/ml) (Gemini Bio Products) and selected for 6 days. After puromycin selection, cells were plated at a density of one cell per well into 96-well plates to isolate individual clones. Disruption of the *STIM1* or *STIM2* genes was confirmed in individual clones through Sanger sequencing, Western blot analysis, and functional Ca^{2+} imaging experiments.

Single cell Ca^{2+} imaging

HEK293 and HCT116 cells were seeded on 25-mm glass coverslips overnight, mounted in Attofluor cell chambers (Thermo Fisher Scientific), and incubated in Dulbeccos modified Eagle's or McCoy's media containing 2 μM Fura-2AM (Molecular Probes) at 37 °C for 30 min as described previously (56, 58). Following loading with Fura-2AM, cells were washed three times and incubated for 10 min in a HEPES-buffered saline solution containing the following components: 140 mM NaCl, 1.13 mM $MgCl_2$, 4.7 mM KCl, 2 mM $CaCl_2$, 10 mM D-glucose, and 10 mM HEPES with pH adjusted to 7.4. Chambers were mounted onto a Nikon TS100 inverted microscope equipped with a ×20 Fluor objective and fluorescence images were recorded with a digital fluorescence imaging system (InCytIm2, Intracellular Imaging Inc.). Ca^{2+} imaging was also performed on a Leica DMi8 fluorescence microscope controlled by Leica Application Suite X (Leica). Fura-2AM fluorescence was measured every 2 s by alternative excitation at 340 (F_{340}) and 380 nm (F_{380}) and emission fluorescence was collected at 510 nm. Cytosolic Ca^{2+} concentrations are represented as the ratio of F_{340}/F_{380}. All Ca^{2+} imaging experiments were performed at room temperature and traces are shown as mean ± S.E. from at least three independent experiments.

Western blotting

Cell lines were harvested, washed once with chilled PBS, and lysed in pre-chilled RIPA buffer (Sigma) containing Halt Protease and Phosphatase Inhibitor Mixture (Thermo Fisher Scientific) for 10 min on ice. Samples were centrifuged at 14,000 × *g*, at 4 °C for 10 min and clarified protein supernatants were quantified with the Pierce BCA Protein Assay Kit (Thermo Fisher Scientific). 25 μg of protein extract was loaded on a 4–12% gel NuPAGE BisTris gel (Life Technologies) and transferred to a polyvinylidene difluoride membrane using a Trans-Blot Turbo Transfer System (Bio-Rad). Membranes were blocked in Odyssey Blocking Buffer (LI-COR) for 1 h at room temperature and incubated overnight at 4 °C with one of the following primary antibodies: STIM1 antibody (1:2000; number 4916, Cell Signaling Technology), STIM2 (1:1000; number 4917, Cell Signaling Technology), or GAPDH (1:4000; MAB374, Sigma). Membranes were washed 3 times in 0.1% TBST and incubated for 1 h at room temperature with the following secondary antibodies: IRDye 680RD goat anti-mouse (1:10,000 LI-COR) or IRDye

800RD donkey anti-rabbit (1:10,000 LI-COR). Following 3 washes in 0.1% TBST, membranes were imaged on an Odyssey CLx Imaging System (LI-COR). Western blotting image analysis was performed in Image Studio version 5.2 (LI-COR) and ImageJ.

Förster resonance energy transfer (FRET) measurements

Measurement of OASF FRET sensors was performed on a Leica DMI 6000B inverted automated fluorescence microscope with CFP (438 excitation/483 emission), YFP (500 excitation/542 emission), and FRET (438 excitation/542 emission) filter cubes. Images were acquired every 20 s with each filter cube with a ×40 oil objective and analyzed using Slidebook 6.0 software (Intelligent Imaging Innovations). Exposure times for each channel were: 1000 ms (CFP), 250 ms (YFP), and 1000 ms (FRET). Three channel corrected FRET was calculated with,

$$FC = I_{DA} - Fd/Dd \times I_{DD} - Fa/D_a \times I_{AA} \quad \text{(Eq. 1)}$$

for this formula, I_{DD}, I_{AA}, and I_{DA} are the intensity of the background-subtracted CFP, YFP, and FRET images, respectively. For FRET analysis of OASF sensors, YFP-OASF-YFP and CFP-OASF-CFP were used for calculation of correction images and bleed through of CFP and YFP through the FRET filter. For analysis of OASF2 sensors, YFP-OASF2-YFP and CFP-OASF2-CFP were used for correction images. The E-FRET method to analyze 3-cube FRET images as initially described by Zal and Gascoigne (59) was calculated with the following formula.

$$E_{app} = F_c/(FC + G \times I_{DD}) \quad \text{(Eq. 2)}$$

All FRET experiments were performed by transient transfection of OASF/OASF2 constructs into HEK293 STIM1/STIM2 double knockout cells.

Statistics

All data analyses were performed with GraphPad Prism 8 (GraphPad Software) and data are presented as mean ± S.E. An unpaired, nonparametric Mann-Whitney test was used for statistical comparisons between two groups and the Kruskal-Wallis test with Dunn's multiple comparisons was used for comparison between multiple groups.

Author contributions—S. M. E., R. E. Y., and M. T. conceptualization; S. M. E. and R. E. Y. data curation; S. M. E. and R. E. Y. formal analysis; S. M. E., R. E. Y., N. H., and M. T. validation; S. M. E., R. E. Y., P. X., and X. Z. investigation; S. M. E., R. E. Y., and M. T. visualization; S. M. E., R. E. Y., P. X., X. Z., T. P., R. N., and M. G. methodology; S. M. E. and M. T. writing-original draft; R. E. Y., I. S. A., N. H., K. M., D. L. G., and M. T. writing-review and editing; P. X., R. N., K. P. S., Y. Z., I. S. A., N. H., K. M., and D. L. G. resources; M. T. supervision; M. T. funding acquisition; M. T. project administration.

References

1. Putney, J. W., Jr. (1986) A model for receptor-regulated calcium entry. *Cell Calcium* **7,** 1–12 CrossRef Medline
2. Prakriya, M., and Lewis, R. S. (2015) Store-operated calcium channels. *Physiol. Rev.* **95,** 1383–1436 CrossRef Medline
3. Trebak, M., and Putney, J. W., Jr. (2017) ORAI calcium channels. *Physiology (Bethesda)* **32,** 332–342 CrossRef Medline
4. Fahrner, M., Schindl, R., Muik, M., Derler, I., and Romanin, C. (2017) The STIM-Orai pathway: the interactions between STIM and Orai. *Adv. Exp. Med. Biol.* **993,** 59–81 CrossRef Medline
5. Trebak, M., and Kinet, J. P. (2019) Calcium signalling in T cells. *Nat. Rev. Immunol.* **19,** 154–169 CrossRef Medline
6. Wang, X., Wang, Y., Zhou, Y., Hendron, E., Mancarella, S., Andrake, M. D., Rothberg, B. S., Soboloff, J., and Gill, D. L. (2014) Distinct Orai-coupling domains in STIM1 and STIM2 define the Orai-activating site. *Nat. Commun.* **5,** 3183 CrossRef Medline
7. Zhou, Y., Cai, X., Nwokonko, R. M., Loktionova, N. A., Wang, Y., and Gill, D. L. (2017) The STIM-Orai coupling interface and gating of the Orai1 channel. *Cell Calcium* **63,** 8–13 CrossRef Medline
8. Zhou, Y., Wang, X., Wang, X., Loktionova, N. A., Cai, X., Nwokonko, R. M., Vrana, E., Wang, Y., Rothberg, B. S., and Gill, D. L. (2015) STIM1 dimers undergo unimolecular coupling to activate Orai1 channels. *Nat. Commun.* **6,** 8395 CrossRef Medline
9. Luik, R. M., Wang, B., Prakriya, M., Wu, M. M., and Lewis, R. S. (2008) Oligomerization of STIM1 couples ER calcium depletion to CRAC channel activation. *Nature* **454,** 538–542 CrossRef Medline
10. Stathopulos, P. B., Li, G. Y., Plevin, M. J., Ames, J. B., and Ikura, M. (2006) Stored Ca^{2+} depletion-induced oligomerization of stromal interaction molecule 1 (STIM1) via the EF-SAM region: an initiation mechanism for capacitive Ca^{2+} entry. *J. Biol. Chem.* **281,** 35855–35862 CrossRef Medline
11. Brandman, O., Liou, J., Park, W. S., and Meyer, T. (2007) STIM2 is a feedback regulator that stabilizes basal cytosolic and endoplasmic reticulum Ca^{2+} levels. *Cell* **131,** 1327–1339 CrossRef Medline
12. Parvez, S., Beck, A., Peinelt, C., Soboloff, J., Lis, A., Monteilh-Zoller, M., Gill, D. L., Fleig, A., and Penner, R. (2008) STIM2 protein mediates distinct store-dependent and store-independent modes of CRAC channel activation. *FASEB J.* **22,** 752–761 CrossRef Medline
13. Zhou, Y., Mancarella, S., Wang, Y., Yue, C., Ritchie, M., Gill, D. L., and Soboloff, J. (2009) The short N-terminal domains of STIM1 and STIM2 control the activation kinetics of Orai1 channels. *J. Biol. Chem.* **284,** 19164–19168 CrossRef Medline
14. Zheng, S., Ma, G., He, L., Zhang, T., Li, J., Yuan, X., Nguyen, N. T., Huang, Y., Zhang, X., Gao, P., Nwokonko, R., Gill, D. L., Dong, H., Zhou, Y., and Wang, Y. (2018) Identification of molecular determinants that govern distinct STIM2 activation dynamics. *PLoS Biol.* **16,** e2006898 CrossRef Medline
15. Yuan, J. P., Zeng, W., Dorwart, M. R., Choi, Y. J., Worley, P. F., and Muallem, S. (2009) SOAR and the polybasic STIM1 domains gate and regulate Orai channels. *Nat. Cell Biol.* **11,** 337–343 CrossRef Medline
16. Abdullaev, I. F., Bisaillon, J. M., Potier, M., Gonzalez, J. C., Motiani, R. K., and Trebak, M. (2008) Stim1 and Orai1 mediate CRAC currents and store-operated calcium entry important for endothelial cell proliferation. *Circ. Res.* **103,** 1289–1299 CrossRef Medline
17. Potier, M., Gonzalez, J. C., Motiani, R. K., Abdullaev, I. F., Bisaillon, J. M., Singer, H. A., and Trebak, M. (2009) Evidence for STIM1- and Orai1-dependent store-operated calcium influx through ICRAC in vascular smooth muscle cells: role in proliferation and migration. *FASEB J.* **23,** 2425–2437 CrossRef Medline
18. Ong, H. L., de Souza, L. B., Zheng, C., Cheng, K. T., Liu, X., Goldsmith, C. M., Feske, S., and Ambudkar, I. S. (2015) STIM2 enhances receptor-stimulated Ca^{2+} signaling by promoting recruitment of STIM1 to the endoplasmic reticulum-plasma membrane junctions. *Sci. Signal.* **8,** ra3 CrossRef Medline
19. Subedi, K. P., Ong, H. L., Son, G. Y., Liu, X., and Ambudkar, I. S. (2018) STIM2 induces activated conformation of STIM1 to control Orai1 function in ER-PM junctions. *Cell Rep.* **23,** 522–534 CrossRef Medline
20. Jairaman, A., and Prakriya, M. (2013) Molecular pharmacology of store-operated CRAC channels. *Channels* (*Austin*) **7,** 402–414 CrossRef Medline
21. Tian, C., Du, L., Zhou, Y., and Li, M. (2016) Store-operated CRAC channel inhibitors: opportunities and challenges. *Future Med. Chem.* **8,** 817–832 CrossRef Medline

22. Schindl, R., Bergsmann, J., Frischauf, I., Derler, I., Fahrner, M., Muik, M., Fritsch, R., Groschner, K., and Romanin, C. (2008) 2-Aminoethoxydiphenyl borate alters selectivity of Orai3 channels by increasing their pore size. *J. Biol. Chem.* **283,** 20261–20267 CrossRef Medline
23. Lis, A., Peinelt, C., Beck, A., Parvez, S., Monteilh-Zoller, M., Fleig, A., and Penner, R. (2007) CRACM1, CRACM2, and CRACM3 are store-operated Ca^{2+} channels with distinct functional properties. *Curr. Biol.* **17,** 794–800 CrossRef Medline
24. Wang, Y., Deng, X., Zhou, Y., Hendron, E., Mancarella, S., Ritchie, M. F., Tang, X. D., Baba, Y., Kurosaki, T., Mori, Y., Soboloff, J., and Gill, D. L. (2009) STIM protein coupling in the activation of Orai channels. *Proc. Natl. Acad. Sci. U.S.A.* **106,** 7391–7396 CrossRef Medline
25. Prakriya, M., and Lewis, R. S. (2001) Potentiation and inhibition of Ca^{2+} release-activated Ca^{2+} channels by 2-aminoethyldiphenyl borate (2-APB) occurs independently of IP_3 receptors. *J. Physiol.* **536,** 3–19 CrossRef Medline
26. DeHaven, W. I., Smyth, J. T., Boyles, R. R., Bird, G. S., and Putney, J. W., Jr. (2008) Complex actions of 2-aminoethyldiphenyl borate on store-operated calcium entry. *J. Biol. Chem.* **283,** 19265–19273 CrossRef Medline
27. Peinelt, C., Lis, A., Beck, A., Fleig, A., and Penner, R. (2008) 2-Aminoethoxydiphenyl borate directly facilitates and indirectly inhibits STIM1-dependent gating of CRAC channels. *J. Physiol.* **586,** 3061–3073 CrossRef Medline
28. Wei, M., Zhou, Y., Sun, A., Ma, G., He, L., Zhou, L., Zhang, S., Liu, J., Zhang, S. L., Gill, D. L., and Wang, Y. (2016) Molecular mechanisms underlying inhibition of STIM1-Orai1-mediated Ca^{2+} entry induced by 2-aminoethoxydiphenyl borate. *Pflugers Arch.* **468,** 2061–2074 CrossRef Medline
29. Zhang, S. L., Kozak, J. A., Jiang, W., Yeromin, A. V., Chen, J., Yu, Y., Penna, A., Shen, W., Chi, V., and Cahalan, M. D. (2008) Store-dependent and -independent modes regulating Ca^{2+} release-activated Ca^{2+} channel activity of human Orai1 and Orai3. *J. Biol. Chem.* **283,** 17662–17671 CrossRef Medline
30. Motiani, R. K., Abdullaev, I. F., and Trebak, M. (2010) A novel native store-operated calcium channel encoded by Orai3: selective requirement of Orai3 *versus* Orai1 in estrogen receptor-positive versus estrogen receptor-negative breast cancer cells. *J. Biol. Chem.* **285,** 19173–19183 CrossRef Medline
31. Yamashita, M., Somasundaram, A., and Prakriya, M. (2011) Competitive modulation of Ca^{2+} release-activated Ca^{2+} channel gating by STIM1 and 2-aminoethyldiphenyl borate. *J. Biol. Chem.* **286,** 9429–9442 CrossRef Medline
32. Trebak, M., Bird, G. S., McKay, R. R., and Putney, J. W., Jr. (2002) Comparison of human TRPC3 channels in receptor-activated and store-operated modes: differential sensitivity to channel blockers suggests fundamental differences in channel composition. *J. Biol. Chem.* **277,** 21617–21623 CrossRef Medline
33. Li, M., Jiang, J., and Yue, L. (2006) Functional characterization of homo- and heteromeric channel kinases TRPM6 and TRPM7. *J. Gen. Physiol.* **127,** 525–537 CrossRef Medline
34. Hu, H. Z., Gu, Q., Wang, C., Colton, C. K., Tang, J., Kinoshita-Kawada, M., Lee, L. Y., Wood, J. D., and Zhu, M. X. (2004) 2-Aminoethoxydiphenyl borate is a common activator of TRPV1, TRPV2, and TRPV3. *J. Biol. Chem.* **279,** 35741–35748 CrossRef Medline
35. Zhou, Y., Nwokonko, R. M., Cai, X., Loktionova, N. A., Abdulqadir, R., Xin, P., Niemeyer, B. A., Wang, Y., Trebak, M., and Gill, D. L. (2018) Cross-linking of Orai1 channels by STIM proteins. *Proc. Natl. Acad. Sci. U.S.A.* **115,** E3398–E3407 CrossRef Medline
36. Stathopulos, P. B., and Ikura, M. (2013) Structural aspects of calcium-release activated calcium channel function. *Channels (Austin)* **7,** 344–353 CrossRef Medline
37. Muik, M., Fahrner, M., Schindl, R., Stathopulos, P., Frischauf, I., Derler, I., Plenk, P., Lackner, B., Groschner, K., Ikura, M., and Romanin, C. (2011) STIM1 couples to ORAI1 via an intramolecular transition into an extended conformation. *EMBO J.* **30,** 1678–1689 CrossRef Medline
38. Lunz, V., Romanin, C., and Frischauf, I. (2019) STIM1 activation of Orai1. *Cell Calcium* **77,** 29–38 Medline
39. Derler, I., Jardin, I., and Romanin, C. (2016) Molecular mechanisms of STIM/Orai communication. *Am. J. Physiol. Cell Physiol.* **310,** C643–C662 CrossRef Medline
40. Muik, M., Fahrner, M., Derler, I., Schindl, R., Bergsmann, J., Frischauf, I., Groschner, K., and Romanin, C. (2009) A cytosolic homomerization and a modulatory domain within STIM1 C terminus determine coupling to ORAI1 channels. *J. Biol. Chem.* **284,** 8421–8426 CrossRef Medline
41. Yu, F., Sun, L., Courjaret, R., and Machaca, K. (2011) Role of the STIM1 C-terminal domain in STIM1 clustering. *J. Biol. Chem.* **286,** 8375–8384 CrossRef Medline
42. Yu, F., Sun, L., Hubrack, S., Selvaraj, S., and Machaca, K. (2013) Intramolecular shielding maintains the ER Ca^{2+} sensor STIM1 in an inactive conformation. *J. Cell Sci.* **126,** 2401–2410 CrossRef Medline
43. Miederer, A. M., Alansary, D., Schwär, G., Lee, P. H., Jung, M., Helms, V., and Niemeyer, B. A. (2015) A STIM2 splice variant negatively regulates store-operated calcium entry. *Nat. Commun* **6,** 6899 CrossRef Medline
44. Rana, A., Yen, M., Sadaghiani, A. M., Malmersjö, S., Park, C. Y., Dolmetsch, R. E., and Lewis, R. S. (2015) Alternative splicing converts STIM2 from an activator to an inhibitor of store-operated calcium channels. *J. Cell Biol.* **209,** 653–669 CrossRef Medline
45. Zheng, L., Stathopulos, P. B., Schindl, R., Li, G. Y., Romanin, C., and Ikura, M. (2011) Auto-inhibitory role of the EF-SAM domain of STIM proteins in store-operated calcium entry. *Proc. Natl. Acad. Sci. U.S.A.* **108,** 1337–1342 CrossRef Medline
46. Bhardwaj, R., Müller, H. M., Nickel, W., and Seedorf, M. (2013) Oligomerization and Ca^{2+}/calmodulin control binding of the ER Ca^{2+}-sensors STIM1 and STIM2 to plasma membrane lipids. *Biosci. Rep.* **33,** e00077 Medline
47. Nelson, H. A., Leech, C. A., Kopp, R. F., and Roe, M. W. (2018) Interplay between ER Ca^{2+} binding proteins, STIM1 and STIM2, is required for store-operated Ca^{2+} entry. *Int. J. Mol. Sci.* **19,** e1522 Medline
48. Berna-Erro, A., Braun, A., Kraft, R., Kleinschnitz, C., Schuhmann, M. K., Stegner, D., Wultsch, T., Eilers, J., Meuth, S. G., Stoll, G., and Nieswandt, B. (2009) STIM2 regulates capacitive Ca^{2+} entry in neurons and plays a key role in hypoxic neuronal cell death. *Sci. Signal.* **2,** ra67 Medline
49. Gruszczynska-Biegala, J., Pomorski, P., Wisniewska, M. B., and Kuznicki, J. (2011) Differential roles for STIM1 and STIM2 in store-operated calcium entry in rat neurons. *PLoS ONE* **6,** e19285 CrossRef Medline
50. Sun, S., Zhang, H., Liu, J., Popugaeva, E., Xu, N. J., Feske, S., White, C. L., 3rd, and Bezprozvanny, I. (2014) Reduced synaptic STIM2 expression and impaired store-operated calcium entry cause destabilization of mature spines in mutant presenilin mice. *Neuron* **82,** 79–93 CrossRef Medline
51. Popugaeva, E., Pchitskaya, E., Speshilova, A., Alexandrov, S., Zhang, H., Vlasova, O., and Bezprozvanny, I. (2015) STIM2 protects hippocampal mushroom spines from amyloid synaptotoxicity. *Mol. Neurodegener.* **10,** 37 CrossRef Medline
52. Pchitskaya, E., Kraskovskaya, N., Chernyuk, D., Popugaeva, E., Zhang, H., Vlasova, O., and Bezprozvanny, I. (2017) Stim2-Eb3 association and morphology of dendritic spines in hippocampal neurons. *Sci. Rep.* **7,** 17625 CrossRef Medline
53. Bittremieux, M., Gerasimenko, J. V., Schuermans, M., Luyten, T., Stapleton, E., Alzayady, K. J., De Smedt, H., Yule, D. I., Mikoshiba, K., Vangheluwe, P., Gerasimenko, O. V., Parys, J. B., and Bultynck, G. (2017) DPB162-AE, an inhibitor of store-operated Ca^{2+} entry, can deplete the endoplasmic reticulum Ca^{2+} store. *Cell Calcium* **62,** 60–70 CrossRef Medline
54. Hendron, E., Wang, X., Zhou, Y., Cai, X., Goto, J., Mikoshiba, K., Baba, Y., Kurosaki, T., Wang, Y., and Gill, D. L. (2014) Potent functional uncoupling between STIM1 and Orai1 by dimeric 2-aminodiphenyl borinate analogs. *Cell Calcium* **56,** 482–492 CrossRef Medline
55. Goto, J., Suzuki, A. Z., Ozaki, S., Matsumoto, N., Nakamura, T., Ebisui, E., Fleig, A., Penner, R., and Mikoshiba, K. (2010) Two novel 2-aminoethyl diphenylborinate (2-APB) analogues differentially activate and inhibit store-operated Ca^{2+} entry via STIM proteins. *Cell Calcium* **47,** 1–10 CrossRef Medline
56. Zhang, X., González-Cobos, J. C., Schindl, R., Muik, M., Ruhle, B., Motiani, R. K., Bisaillon, J. M., Zhang, W., Fahrner, M., Barroso, M., Matrougui, K., Romanin, C., and Trebak, M. (2013) Mechanisms of STIM1 activation of

store-independent leukotriene C4-regulated Ca^{2+} channels. *Mol. Cell. Biol.* **33,** 3715–3723 CrossRef Medline

57. Zhang, X., Zhang, W., González-Cobos, J. C., Jardin, I., Romanin, C., Matrougui, K., and Trebak, M. (2014) Complex role of STIM1 in the activation of store-independent Orai1/3 channels. *J. Gen. Physiol.* **143,** 345–359 CrossRef Medline
58. Desai, P. N., Zhang, X., Wu, S., Janoshazi, A., Bolimuntha, S., Putney, J. W., and Trebak, M. (2015) Multiple types of calcium channels arising from alternative translation initiation of the Orai1 message. *Sci. Signal.* **8,** ra74 CrossRef Medline
59. Zal, T., and Gascoigne, N. R. (2004) Photobleaching-corrected FRET efficiency imaging of live cells. *Biophys. J.* **86,** 3923–3939 CrossRef Medline